Optimal deployments of UAVs with directional antennas for a power-efficient coverage

Jun Guo, Philipp Walk, and Hamid Jafarkhani
Center for Pervasive Communications and Computing
University of California, Irvine, CA 92697-2625
{guoj4,pwalk,hamidj}@uci.edu

***Abstract*—To provide a reliable wireless uplink for users in a given ground area, one can deploy Unmanned Aerial Vehicles (UAVs) as base stations (BSs). In another application, one can use UAVs to collect data from sensors on the ground. For a power-efficient and scalable deployment of such flying BSs, directional antennas can be utilized to efficiently cover arbitrary 2-D ground areas. We consider a large-scale wireless path-loss model with a realistic angle-dependent radiation pattern for the directional antennas. Based on such a model, we determine the optimal 3-D deployment of N UAVs to minimize the average transmit-power consumption of the users in a given target area. The users are assumed to have identical transmitters with ideal omnidirectional antennas and the UAVs have identical directional antennas with given half-power beamwidth (HPBW) and symmetric radiation pattern along the vertical axis. For uniformly distributed ground users, we show that the UAVs have to share a common flight height in an optimal power-efficient deployment, by simulations. We also derive in closed-form the asymptotic optimal common flight height of N UAVs in terms of the area size, data-rate, bandwidth, HPBW, and path-loss exponent.**

***Index Terms*—Node deployment, UAVs, directional antennas, power optimization**

I. Introduction

Due to the decreasing production cost of Unmanned Aerial Vehicles (UAVs), wireless communication coverage for large areas can be achieved efficiently and flexibly by using a network of UAVs equipped with wireless transceivers [2]–[5]. These UAVs can communicate to each other or to nearby stationary base stations and operate as a relay network for users on the ground [6], [7]. To improve wireless links to the users, such flying base stations (BSs) use directional antennas to concentrate the radiation power to smaller cells on the ground. Hence, directional antennas reduce power consumption and interference with neighboring cells [8]–[13]. It is common to assume that the antenna pattern of a directional antenna is an ideal beam and symmetric in the azimuth plane. In such a model, the radiation intensity is constant for elevation angles inside the beam, defined by its beamwidth, and zero or small outside [11]–[15]. Such an approximation is sufficient for high-altitude UAVs where the ground cells can be covered uniformly by a small fraction of the beamwidth. But, when the same number of UAVs needs to cover the same cells at a lower altitude, they require the whole beamwidth or even more, which for realistic directional antennas does not result in a constant radiation pattern. Moreover, the objective is to find the maximum cell-radius which guarantees a reliable downlink at a given data-rate (coverage). Using the Shannon capacity formula, for a given bandwidth and noise power, this reduces to a minimum required receive power at the UAV for each ground user equipment (UE) [16]. To cover a given target area at the ground, efficiently with N identical UAVs, an optimal common height is determined. Because of the circular cell shapes, this approach, does not result in a full coverage of the target area if the cells do not overlap or in an inefficient full coverage if the cells overlap. By focusing on an uplink coverage and a more realistic model, our approach is slightly different. UEs can adjust their transmit powers to achieve a reliable uplink connection in a given range and at a given data-rate. Therefore, we consider a full coverage model by using a transmit-power model which is continuous in the elevation angle and hence continuous in the UE positions. Assuming the UEs are distributed by a given density function in a given ground area and for a given uplink data-rate, the objective for an optimal UAV deployment is then to minimize the average transmit-power over all UEs in the target area [1], [17], [18]. The target area can have any polygonal shape which can be fully covered by any number of UAVs.

To achieve our goal, we use a more realistic directional antenna pattern, which considers a continuous angle-dependent radiation gain. The impact of antenna radiation patterns on the UAV coverage performance is well studied in [19]. Our recent conference paper introduced a similar concept for 2-D UAV deployments to cover 1-D ground areas [1]. The received UAV power depends on the line-of-sight (LoS) distance between the UAV and the corresponding ground user and the UAV's antenna gain at the corresponding Angle of Arrival (AoA). As shown in Fig. 1, the AoA θ is the arc-cosine of the ratio of the height and the LoS distance. In this paper, we extend the model to 3-D deployments and adjustable beamwidths. We model the antenna gain by various cosine-powers of the radiation angle (AoA) [20], [21]. To minimize the average transmit power of UEs in a 2-D ground area, by deploying N UAVs, a continuous $N-$facility locational optimization problem has to be solved. This can also be seen as an $N-$point parameterized quantization problem, where the N UAV ground positions are the reproduction points and the N ground cells are the quantization regions of the target area. The goal is to find the optimal quantizer (UAV deployment) which minimizes the distortion measure, given by the average transmit-power

This work was supported in part by the NSF Award CCF-1815339. Part of the work was presented in Data Compression Conference [1].

of the UEs, in a given target area. We assume that only one UE per cell communicates at each time, as in a time-division multiple-access (TDMA) system. This problem has been investigated for example in [18], [22]–[24] by assuming a given common UAV height and an ideal beam. In this work, we investigate the UAV optimization problem over all possible ground locations in the target area and heights. This results in a 3-D optimization problem with a power function parameterized by the UAV heights. Such a parameterized cost function can also be used to formulate heterogeneous sensor deployment problems, as for example investigated in [24]. In many applications, as in sensor or vehicle deployments, the optimal weights and parameters of the system are usually unknown, but adjustable. Therefore, one wishes to optimize the deployment over all admissible parameter values [25]. In this work, for a large number of UAVs, we derive the closed-form optimal deployments to serve users uniformly distributed in a given 2-D target area. For given arbitrary flight heights, the optimal regions (cells) are known to be generalized Voronoi (Möbius) regions, which can be non-convex and disconnected sets [26]. A deployment optimization over arbitrary heights constitutes a heterogeneous problem whose solution is not known in a closed-form [23]. However, our numerical solutions show that asymptotically a common height is optimal.

A dual problem is a downlink scenario, which minimizes the UAVs' average transmit-power to cover UEs at a given average downlink-rate [15]. Our uplink UAV deployment solution is also optimal for the downlink problem. The contributions of the paper can be summarized as:

- We consider a more realistic directional antenna model that considers a continuous angle-dependent radiation gain.
- We investigate the optimal 3-D UAV deployment problem over all possible ground locations and flight heights to minimize the total average transmit-power.
- We show numerically that the global optimal deployment is asymptotically given by a hexagonal lattice of the UAV ground positions and a unique common flight height.

The rest of the paper is organized as follows: We introduce a realistic and mathematically tractable wireless communication model for ground users to UAVs with directional antennas in Section II. We formulate and solve the optimal 3-D UAV deployment problem over given arbitrary ground areas in Section III. In Section IV, we provide iterative Lloyd-like algorithms to derive UAV deployments for various parameters with uniform and non-uniform user distributions. In Section V, we provide simulation results to compare to other deployments derived in [13], [18] and verify the asymptotic optimality of common height deployments. Finally, we provide conclusions in Section VI.

a) Notation: We denote the first N natural numbers, $\mathbb{N}$, by $[N] = \{1, 2, \ldots, N\}$. We write real numbers in $\mathbb{R}$ by small letters and row vectors by bold letters. The Euclidean norm of $\mathbf{x}$ is given by $\|\mathbf{x}\| = \sqrt{\sum_n x_n^2}$. We denote by $\mathcal{V}^c$ the complement of the set $\mathcal{V} \subset \mathbb{R}^d$. The real numbers larger than some $a \geq 0$ are denoted by $\mathbb{R}_a$.

II. System model

We investigate the 3-D deployment of N UAVs positioned in $\Omega \times \mathbb{R}_0$, operating as flying BSs to provide a wireless communication link to UEs in a given 2-D target region $\Omega \subset \mathbb{R}^2$ on the ground. Here, the nth UAV's position, $(\mathbf{q}_n, h_n)$, is given by its ground position $\mathbf{q}_n = (x_n, y_n) \in \Omega$ and its height $h_n \in \mathbb{R}_0$. The optimal UAV deployment is then defined by the minimum average transmit-power to provide an uplink connection for UEs, distributed by a continuous density function λ in Ω. Each UE selects the UAV which requires the smallest transmit-power[1]. This results in a so called generalized Voronoi (user) region for each UAV and partitions Ω into N user regions. Hence, the optimal average-power deployment problem of N UAVs is similar to an $N-$point quantization problem, as defined in [1], [17], [18], [22], [23], [25], [27]–[30]. For homogeneous deployments, where the BSs are mounted on the ground or at a fixed common height, the Voronoi regions for a large number of BSs converge to the well-known hexagonal regions [31]. For heterogeneous BSs or different heights, the optimal regions are unknown [23].

Recently, UAVs with directional antennas have been widely studied in the literature to increase the efficiency of wireless links [8]–[14], [32]. Usually, the antenna gain in a given direction is approximated by a constant gain $\bar{G}_{\text{HPBW}}$ within a 3dB beamwidth θ_{HPBW}, called the half-power-beam-width (HPBW), and by zero or a small value outside the beamwidth, resulting in an ideal directional antenna pattern (radiation intensity or directional gain)

$$G_{\text{HPBW}}(\theta) = G_{\text{HPBW}}(\theta, \phi) = \begin{cases} \bar{G}_{\text{HPBW}}, & |\theta| \leq \theta_{\text{HPBW}}/2 \\ 0, & \text{else} \end{cases}, \theta \in [0, \pi], \phi \in [0, 2\pi], \quad (1)$$

which is independent of the azimuth angle ϕ and depends only on the radiation angle θ or elevation angle $\theta_E = \pi/2 - \theta$, see also Fig. 1. Hence, the antenna pattern is symmetric in the azimuth plane. The gain $\bar{G}_{\text{HPBW}}$ describes the average directional gain over the main lobe. However, definition (1) ignores the strong angle-dependent gain of directional antennas [20]. Since, due to the flight zone restrictions of aircrafts, the maximum heights for UAVs are typically less than 1000m, such an angle-dependent gain becomes crucial if a few UAVs need to cover large target areas. As shown in Fig. 1, to obtain a more realistic uplink model, we consider an antenna gain that depends continuously on the actual radiation angle or angle of destination (AoD) $\theta_n(\boldsymbol{\omega}) \in [0, \frac{\pi}{2}]$ from the nth UAV at $\mathbf{p}_n = (\mathbf{q}_n, h_n) \in \Omega \times \mathbb{R}_0$ to a UE at $\boldsymbol{\omega} = (x, y) \in \Omega = [0, 10]^2$. We denote by $\theta_{E,n}(\boldsymbol{\omega})$ the elevation angle or angle of arrival (AoA). To capture the power fall-off versus the LoS distance d_n along with the random attenuation due to shadowing, we adopt the following model [33, (2.51)]

$$PL_{dB} = 10 \log_{10} K - 10\alpha \log_{10}(d_n/d_0) - \psi_{dB}, \quad (2)$$

where K is a unit-less constant depending on the antenna

[1]We assume an orthogonal communication by using frequency or time separation (slotted protocols) with no inter-user interference.

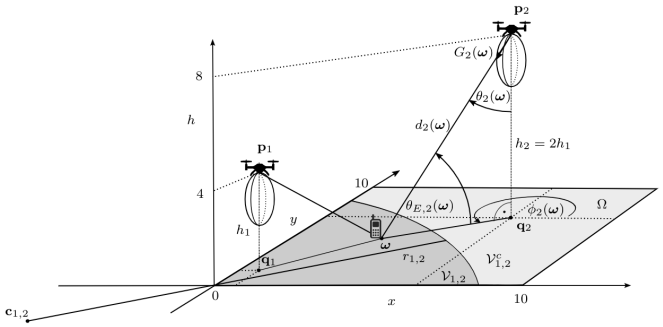

Fig. 1: UAV deployment with directional antenna gains and associated UE cells with path-loss $\alpha = 2$, antenna parameter $\kappa = 1$, and $N = 2$ UAVs for a uniform UE distribution in $\Omega = [0, 1]^2$.

characteristics and frequency, d_0 is a reference distance to the actual distance $d_n > d_0$ at which an exponential path-loss needs to be considered, $\alpha \geq 1$ is the path-loss exponent, and ψ_{dB} is a Gaussian random variable following $\mathcal{N}\left(0, \sigma^2_{\psi_{dB}}\right)$ representing the random channel attenuation (shadowing). This Cellular-to-UAV or terrestrial log-distance path-loss model is widely used and recommended by both 3GPP and ITU [34], [35]. Practical values of α are between 1 and 6. The LoS distance of UE at $\boldsymbol{\omega}$ to the nth UAV at $(\mathbf{q}_n, h_n)$ is given by

$$d_n(\boldsymbol{\omega}) = \sqrt{\|\mathbf{q}_n - \boldsymbol{\omega}\|^2 + h_n^2} = \sqrt{(x_n - x)^2 + (y_n - y)^2 + h_n^2}. \tag{3}$$

Common practical measurements of α have been provided in [35]. With this model, the received power at the nth UAV from a UE at $\boldsymbol{\omega}$ is given by [33]

$$\begin{aligned} P_{\text{RX},n}(\boldsymbol{\omega}) &= P_{\text{TX},n}(\boldsymbol{\omega})\tilde{\beta}_n(\boldsymbol{\omega}) \\ &= P_{\text{TX},n}(\boldsymbol{\omega}) G_{\text{TX}} G_{\text{RX},n}(\boldsymbol{\omega}) K \frac{d_0^\alpha}{d_n^\alpha(\boldsymbol{\omega})} 10^{-\frac{\psi_{dB}}{10}}, \end{aligned} \tag{4}$$

where $\sqrt{\tilde{\beta}_n(\boldsymbol{\omega})}$ is the effective channel attenuation between the UE and the UAV. To derive a realistic channel model, not only do we consider the LoS distance in $\tilde{\beta}_n(\boldsymbol{\omega})$, but also we take into account the corresponding angle between the UE and the UAV. For the UE, the dimensionless transmit antenna gain $G_{\text{TX}} > 0$ is assumed to model a perfect omnidirectional antenna, which is identical for all UEs. The UAVs are equipped with identical directional receive antennas with gains

$$\begin{aligned} G_{\text{RX},n}(\boldsymbol{\omega}, \kappa) &= G_\kappa(\theta_n(\boldsymbol{\omega})) \\ &= D_0(\kappa) \cos^\kappa(\theta_n(\boldsymbol{\omega})) = D_0(\kappa) \frac{h_n^\kappa}{d_n^\kappa(\boldsymbol{\omega})}. \end{aligned} \tag{5}$$

These gains depend on the radiation angle $\theta = \theta_n(\boldsymbol{\omega}) \in [-\pi/2, \pi/2]$ and are symmetric along the vertical direction, i.e., independent of the azimuth angle ϕ, as for example in horn or uniform linear array (ULA) antennas [21, Sec.2.6.1]. Compared to our conference paper [1], we have added an additional antenna parameter $\kappa \geq 1$ to the directional antenna gain which defines the *maximum directivity* of the antenna

$$D_0(\kappa) = \frac{4\pi}{\Omega_A(\kappa)} \geq 1, \tag{6}$$

where $\Omega_A(\kappa)$ denotes the *beam solid angle* [21, (2-23)]. For simplicity, in the antenna pattern $U_\kappa(\theta) = \cos^\kappa(\theta)$, we ignore the l possible minor (side) lobes, which are usually modeled by $\cos(l\theta)$ for a more realistic antenna pattern [20]. We can ignore the side lobes and especially the back lobes ($|\theta| > \pi/2$) since there is no significant reflection above and side-wards the UAVs when they fly at a reasonable flight height, as shown in Fig. 1 and Fig. 2a. In fact, since we are only interested in a power averaged over all user positions in a cell, we essentially average the antenna pattern over all radiation angles which is exactly what (5) describes. To account for the power concentration compared to an ideal isotropic antenna with gain $G_0 = 1$ in each direction, we normalize the symmetric directional antenna gain $G_\kappa(\theta)$ in (5) by the maximal directivity (6), which is inverse proportional to the beam solid angle

$$\begin{aligned} \Omega_A(\kappa) &= \int_0^{2\pi} \int_0^{\pi} U_\kappa(\theta) \sin(\theta) d\theta d\phi \\ &= 2\pi \int_0^{\pi/2} \cos^\kappa(\theta) \sin(\theta) d\theta = \frac{2\pi}{\kappa + 1}, \quad \kappa \geq 1, \end{aligned} \tag{7}$$

where the closed-form expression for the last integral is provided in [36, (2.537.1)]. Combining (6) and (7) results in $D_0(\kappa) = 2(\kappa + 1)$, for $\kappa \geq 1$. Note that we assumed no back-lobe, i.e., $U_k(\theta) = 0$ for $\pi \geq |\theta| \geq \pi/2$. For $\kappa = 0$, we have an isotropic radiation pattern which results in a beam solid angle (no back reflector) $\Omega_A(0) = 4\pi$ and hence to the directivity $D_0(0) = 1$. The directivity of a directional antenna describes the overall power gain, compared to an isotropic antenna, in the direction of maximum gain ($\theta = 0$). The larger κ, the larger the directivity of the directional antenna, and the smaller the beam. Then, large κ's model antennas with small beamwidths and allow to focus (collect) the radiation power in a smaller area on the ground (cell), as shown in [20, Fig. 4] and Fig. 2a. A more insightful antenna parameter is given by the beamwidth θ_{HPBW}. The HPBW is by definition [21] twice the angle $\theta_{\text{HPBW}}/2$ at which the gain is half of the maximum gain, i.e., for the normalized pattern $U_\kappa(\theta_{\text{HPBW}}/2) = 1/2$. Hence, for the pattern $U_\kappa(\theta) = \cos^\kappa(\theta)$, the HPBW relates to κ by

$$\theta_{\text{HPBW}}(\kappa) = 2 \arccos(2^{-1/\kappa}). \tag{8}$$

However, the HPBW only describes the solid angle, in which the gain is at least half the maximum gain $U_\kappa(0)$. The assumption that most of the radiated power is radiated in this solid angle leads to the approximation in (1). Not only does such an approximation neglect the radiation outside the beamwidth, but also it ignores the fact that the continuous radiation pattern monotonically decreases in $|\theta|$ over the range $[-\pi/2, \pi/2]$.

To see the approximation error for a constant directional pattern in (1) versus a cosine pattern (5), we can compare the average powers for uniformly distributed UEs in a circle ground region, covered by a single UAV with beamwidth $\theta_{\text{HPBW}}(\kappa)$ in (8). Here, we only need to adjust $\bar{G}_{\text{HPBW}}$ such that (1) has the same total radiation power as (5), i.e., $\bar{G}_{\text{HPBW}} \int_0^{2\pi} \int_0^{\arccos(2^{-1/\kappa})} \sin(\theta) d\theta d\phi = 4\pi$, which gives $\bar{G}_{\text{HPBW},\kappa} = 2/(1 - 2^{-1/\kappa})$. For a given height h, path-loss exponent α and beamwidth exponent κ, the average received power with cosine-pattern is given by (4) and (5) as

$\bar{P}_{\text{RX}}(h,\kappa,\alpha) = \frac{1}{h\tan(\theta_{\text{HPBW}}(\kappa))}\int_0^{\theta_{\text{HPBW}}(\kappa)} G_\kappa(\theta)h^\alpha/\cos^\alpha(\theta)d\theta$, where we ignored the constant parts. Taking the power ratio of cosine directional gain and constant directional gain results in

$$\rho(\kappa,\alpha)=(\kappa+1)(1-2^{-1/\kappa})\frac{\int_0^{\arccos(2^{-1/\kappa})}\cos^{\kappa-\alpha}(\theta)d\theta}{\int_0^{\arccos(2^{-1/\kappa})}\cos^{-\alpha}(\theta)d\theta}, \quad (9)$$

which is independent of the height (area of the covered circle). This indicates how much a constant antenna gain will bias the optimal average transmit power of the users. For $\kappa=\alpha=2$ in Fig. 2a, the ratio is $\rho(2,2)=0.348$, which corresponds to a 4.6 dB power penalty for the cosine-pattern compared to a constant-pattern.

By using the gain in (5), we have a mathematically tractable model which respects such a continuous angle-dependent radiation gain. Accordingly, the transmit power with random attenuation ψ_{dB} can be rewritten as

$$P_{\text{TX},n}(\boldsymbol{\omega}) = \frac{P_{\text{RX},n}(\boldsymbol{\omega})}{h_n^\kappa K G_{\text{TX}} D_0(\kappa) d_0^\alpha} d_n^{\alpha+\kappa}(\boldsymbol{\omega}) 10^{\frac{\psi_{dB}}{10}}. \quad (10)$$

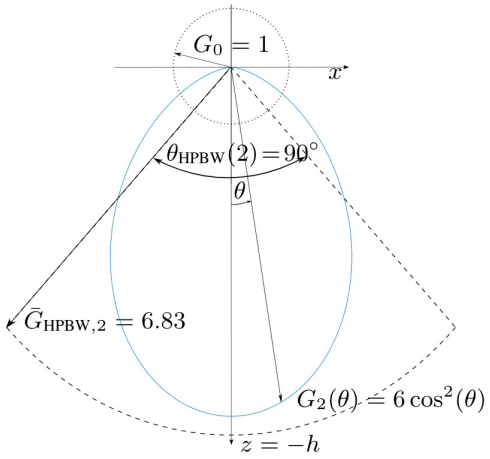

(a)

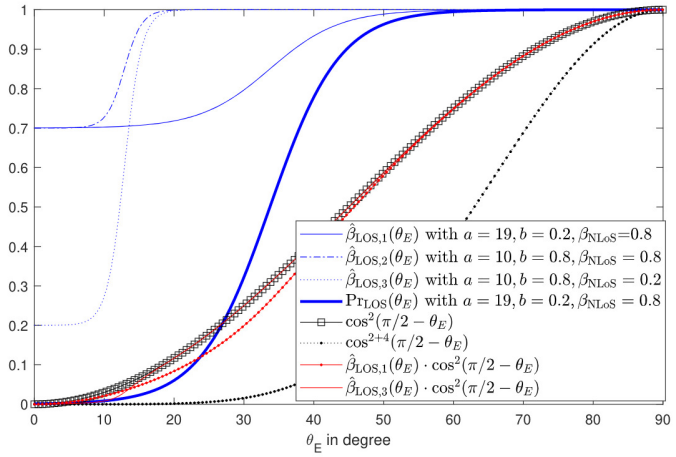

(b)

Fig. 2: (a) Isotropic (dotted), directional with $\kappa=\kappa_{\text{LoS}}=2$ (solid), and constant-beamwidth (dashed) antenna gain (linear) in the elevation plane and normalized to total radiation power 4π. (b) shows the attenuation over the elevation angle θ_{E} for some regularized LoS path-loss parameters versus the cosine antenna pattern with $\kappa_{\text{LoS}}=2$.

The expectation over the random path-loss attenuation ψ_{dB} yields the transmit power

$$P_n(\boldsymbol{\omega})=\mathbb{E}[P_{\text{TX},n}(\boldsymbol{\omega})] = \frac{P_{\text{RX},n}(\boldsymbol{\omega})}{h_n^\kappa K G_{\text{TX}} D_0(\kappa) d_0^\alpha}\cdot \frac{d_n^{\alpha+\kappa}(\boldsymbol{\omega})}{\sqrt{2\pi}\sigma_{\psi_{dB}}}\int_{\mathbb{R}}\exp\left(\ln(10)\frac{\psi_{dB}}{10}-\frac{\psi_{dB}^2}{2\sigma_{\psi_{dB}}^2}\right)d\psi_{dB}. \quad (11)$$

We consider the communication between UE and UAV as reliable if the corresponding bit-rate is at least R_b. Given a channel bandwidth B and noise power N_0, the Shannon formula suggests that $R_b = B\log_2\left(1+\frac{P_{\text{RX},n}}{N_0}\right)$. Therefore, the minimum required received power is $P_0=(2^{R_b/B}-1)N_0$. The minimum transmit power of UE to achieve a minimum received power of P_0 at the nth UAV is then given by

$$P_n(\boldsymbol{\omega}) = P_{\text{TX}}(\mathbf{q}_n, h_n, \boldsymbol{\omega}) = \frac{1}{\beta_0(\alpha)}\cdot\frac{d_n^{\alpha+\kappa}(\boldsymbol{\omega})}{D_0(\kappa)\cdot h_n^\kappa}, \quad (12)$$

where the independent and fixed parameters of the channel attenuation are combined to

$$\beta_0(\alpha)=\frac{K G_{\text{TX}} d_0^\alpha}{P_0}\exp\left(\frac{\sigma_{\psi_{dB}}^2(\ln 10)^2}{200}\right)=\frac{K G_{\text{TX}} d_0^\alpha \sigma_\psi^2}{(2^{\frac{R_b}{B}}-1)N_0}, \quad (13)$$

where σ_ψ^2 is the (linear) average-power of the random shadow attenuation. Hence, $\beta_0(\alpha)$, with unit m^α/W, describes the shadowing, noise-power, bandwidth/data-rate, and the antenna characteristics controlled by the path-loss exponent α. The second factor in (12) is the inverse of the angle and distance-dependent channel/antenna attenuation $\beta_n(\boldsymbol{\omega},\kappa,\alpha) = G_{\text{RX},n}(\boldsymbol{\omega},\kappa)/d_n^\alpha(\boldsymbol{\omega})$, which depends on (5), the directional antenna gain $G_{\text{RX},n}(\boldsymbol{\omega},\kappa)=D_0(\kappa)(h_n/d_n(\boldsymbol{\omega}))^\kappa$ of the nth UAV to a UE at $\boldsymbol{\omega}$, and is the novel part of our model. In this model, the directional antenna gain decreases with the radiation angle and punishes large radiation angles, i.e., UEs with a small elevation angle. A larger κ increases this effect but at the same time provides a larger maximum directivity.

The main goal of this work is to understand the optimal UAV deployment and optimal directional antenna beam for a given user area Ω and number N of UAVs. For the validity of the path-loss model in (2), we need to ensure that $d_n > d_0$ for any UE position $\boldsymbol{\omega}$, which requires a minimum flight height $h_{\min} > d_0$ for each UAV. Such a minimum flight height can also be justified from a security point of view, to prevent collisions of the UAV with objects or people on the ground. Furthermore, a very low UAV height can result in high transmit-powers for far distant UEs, which is not acceptable. As can be seen from (12), the transmit-power P_{TX} is a function of the parameter h_n (UAV flight height) in addition to the ground distance between $\mathbf{q}_n$ (UAV ground position) and $\boldsymbol{\omega}$ (UE position).

So far, we have considered a large-scale fading channel model for Cellular-to-UAV links, in which we have included the angle-dependent directional antenna gain. However, for a ground-user-to-UAV link in an urban area, we also need to consider small-scale fading with Non-LoS (NLoS) paths. Such a NLoS path is due to the blockage of objects on the ground, for example by buildings, trees, or moving vehicles [15], [35], [37], [38]. A NLoS propagation results in a higher path-loss

and hence in an additional attenuation of some $\beta_{\text{NLoS}} \leq 1$. The probability for a LoS propagation can be approximated in the elevation angle $\theta_{\text{E}} = \pi/2 - \theta$ (in radians) by

$$\Pr_{\text{LoS}}(\theta_{\text{E}}) = \frac{1}{1 + ae^{-b(\frac{180}{\pi}\theta_{\text{E}} - a)}}, \tag{14}$$

for some parameters $b > 0$ and $0 < a < 90$ [7], [13], [16]. The probability of a LoS path is monotone increasing in the elevation angle and has an $S-$shaped curve, as shown by the thick blue curve in Fig. 2b. In more dense urban areas, the NLoS paths are more likely, even at larger elevation angles, and the S-curve shifts to the right [16, Fig. 2]. A probabilistic mixing of LoS β_{LoS} and NLoS β_{NLoS} attenuation results in a regularized LoS path-loss given by

$$\begin{aligned}\hat{\beta}_{\text{LoS}}(\theta_{\text{E}}) &= \Pr_{\text{LoS}}(\theta_{\text{E}})\beta_{\text{LoS}} + (1 - \Pr_{\text{LoS}}(\theta_{\text{E}}))\beta_{\text{NLoS}} \\ &= \frac{1 + \beta_{\text{NLoS}} a e^{-b(\frac{180}{\pi}\theta_{\text{E}} - a)}}{1 + ae^{-b(\frac{180}{\pi}\theta_{\text{E}} - a)}},\end{aligned} \tag{15}$$

where we set $\beta_{\text{LoS}} = 1$ and $\beta_{\text{NLoS}} \leq 1$ on the right hand side without loss of generality [7], [38]. We rename the beamwidth exponent to κ_{LoS} to study the effects of LoS and NLoS in Fig. 2. Dividing (12) by the regularized LoS path-loss in (15) provides the required transmit power

$$P_n(\boldsymbol{\omega}) = \frac{1}{\beta_0(\alpha)} \frac{1}{\beta_n(\boldsymbol{\omega}, \kappa_{\text{LoS}}, \alpha)} \frac{1}{\hat{\beta}_{\text{LoS}}(\pi/2 - \theta_n(\boldsymbol{\omega}))}. \tag{16}$$

Since $\beta_n(\boldsymbol{\omega}, \kappa_{\text{LoS}}, \alpha) = d_n^{-\alpha}(\boldsymbol{\omega}) D_0(\kappa_{\text{LoS}}) \cos^{\kappa_{\text{LoS}}}(\theta_n(\boldsymbol{\omega}))$, the angle-dependent component of (16) is $\hat{\beta}_{\text{LoS}}(\pi/2 - \theta) \cdot \cos^{\kappa_{\text{LoS}}}(\theta)$. But since the directional antenna pattern $\cos^{\kappa_{\text{LoS}}}(\theta)$, for some $\kappa_{\text{LoS}} \geq 1$, decays fast to zero if the AoD θ approaches $\pi/2$, the antenna intensity dominates the attenuation gain for large θ. As shown in Fig. 2b, the cosine antenna pattern for $\kappa = \kappa_{\text{LoS}} = 2$ (black square curve) fully absorbs the regularized LoS attenuation of the S-curve (15) for large elevation angles $\theta_E = \pi/2 - \theta$ (red curve). The result is only affected for very small elevation angles (large AoDs). By choosing a proper minimum height $h_{\min}$ for a given area $A = |\Omega|$, small elevation angles can be avoided, such that we can neglect the NLoS path effects. Furthermore, we can also add an additional exponent κ_{NLoS} in the cosine antenna pattern to increase or decrease the descent of the Cosine

$$\begin{aligned}P_n(\boldsymbol{\omega}) &\approx \frac{1}{\beta_0(\alpha) D_0(\kappa_{\text{LoS}})} \frac{d_n^{\alpha}(\boldsymbol{\omega})}{\cos(\theta_n(\boldsymbol{\omega}))^{\kappa_{\text{NLoS}} + \kappa_{\text{LoS}}}} \\ &= \frac{1}{\beta_0(\alpha) D_0(\kappa_{\text{LoS}})} \frac{d_n^{\alpha + \kappa_{\text{NLoS}} + \kappa_{\text{LoS}}}(\boldsymbol{\omega})}{h_n^{\kappa_{\text{NLoS}} + \kappa_{\text{LoS}}}},\end{aligned} \tag{17}$$

which can approximate the regularized LoS path in denser urban areas, as shown in Fig. 2b for $\kappa_{\text{NLoS}} + \kappa_{\text{LoS}} = 4 + 2 = 6$. Note that the maximum directivity only depends on κ_{LoS}. Hence, for fixed $\alpha, \kappa_{\text{LoS}}$, and κ_{NLoS}, a minimization of the average transmit-power for a full coverage of users in Ω results in a 3-D UAV deployment problem that is solved in the next section. For simplicity, from now on, we set $\beta_0(\alpha) D_0(\kappa_{\text{LoS}}) = 1$ ($\text{m}^{\alpha}/\text{W}$) since it does not affect the optimal deployment for fixed $\alpha, \kappa_{\text{LoS}}$. Moreover, in the next section we only consider the constant $\kappa = \kappa_{\text{LoS}} + \kappa_{\text{NLoS}}$.

III. Power-Efficient UAV Deployments

The transmit power (17) defines, with h_n, $\mathbf{q}_n$ and fixed $\alpha, \kappa \geq 1$, a parameter-dependent power function over $\boldsymbol{\omega}$, by identifying $d_n^2(\boldsymbol{\omega}) = \|\boldsymbol{\omega} - \mathbf{q}_n\|^2 + h_n^2$. For a given UE density λ in Ω, UAV deployment $(\mathbf{Q}, \mathbf{h})$ with ground positions $\mathbf{Q} = (\mathbf{q}_1, \ldots, \mathbf{q}_N)$, heights $\mathbf{h} = (h_1, \ldots, h_N)$, and user regions (cells) $\mathcal{R} = \{\mathcal{R}_1, \ldots, \mathcal{R}_N\}$ with $\bigcup \mathcal{R}_n = \Omega$, the average transmit power $\bar{P}$ of each UE in Ω for $\gamma = \frac{\alpha + \kappa}{2} \geq 1$ is given by

$$\begin{aligned}\bar{P}(\mathbf{Q}, \mathbf{h}, \mathcal{R}) &= \sum_{n=1}^{N} \int_{\mathcal{R}_n} P(\boldsymbol{\omega}, \mathbf{q}_n, h_n) \lambda(\boldsymbol{\omega}) d\boldsymbol{\omega} \\ \text{with} \quad P(\boldsymbol{\omega}, \mathbf{q}_n, h_n) &= \frac{(\|\boldsymbol{\omega} - \mathbf{q}_n\|^2 + h_n^2)^{\gamma}}{h_n^{\kappa}}.\end{aligned} \tag{18}$$

Here, we assume that the UE at $\boldsymbol{\omega}$ transmits with the smallest power P to achieve a reliable link to the nearest UAV at $(\mathbf{q}_n, h_n)$. The N regions, which minimize the average transmit power for given ground positions and heights $(\mathbf{Q}, \mathbf{h})$, define a generalized Voronoi tessellation $\mathcal{V} = \{\mathcal{V}_n(\mathbf{Q}, \mathbf{h})\}$ of Ω by

$$\begin{aligned}\bar{P}(\mathbf{Q}, \mathbf{h}) &= \int_{\Omega} \min_{n \in [N]} \{P(\boldsymbol{\omega}, \mathbf{q}_n, h_n)\} \lambda(\boldsymbol{\omega}) d\boldsymbol{\omega} \\ &= \sum_{n=1}^{N} \int_{\mathcal{V}_n(\mathbf{Q}, \mathbf{h})} P(\boldsymbol{\omega}, \mathbf{q}_n, h_n) \lambda(\boldsymbol{\omega}) d\boldsymbol{\omega},\end{aligned} \tag{19}$$

where the *generalized Voronoi regions* $\mathcal{V}_n(\mathbf{Q}, \mathbf{h})$ are defined as the set of sample points (user positions) $\boldsymbol{\omega}$ with smallest power to the nth ground position $\mathbf{q}_n$ with parameter h_n (UAV position). Minimizing the *average transmit-power* $\bar{P}(\mathbf{Q}, \mathbf{h}, \mathcal{V})$ over all UAV positions can be seen as an *$N-$facility locational-parameter optimization problem* [17], [27], [28], [31], [39], where calculating the gradient over a location-dependent integral region $\mathcal{V}_n(\mathbf{Q}, \mathbf{h})$ is the most challenging part. According to the definition of the Voronoi region in (19), we have

$$\begin{aligned}\mathcal{V}_n(\mathbf{Q}, \mathbf{h}) = \{&\boldsymbol{\omega} \in \Omega \mid P(\boldsymbol{\omega}, \mathbf{q}_n, h_n) \\ &\leq P(\boldsymbol{\omega}, \mathbf{q}_m, h_m) \text{ for all } m \neq n\}.\end{aligned} \tag{20}$$

The *minimum average transmit-power* over all possible deployments with minimal flight height $h_{\min}$ is then given by

$$\begin{aligned}\bar{P}^* = \bar{P}(\mathbf{Q}^*, \mathbf{h}^*) &= \min_{(\mathbf{Q}, \mathbf{h}) \in \Omega^N \times \mathbb{R}^N_{h_{\min}}} \bar{P}(\mathbf{Q}, \mathbf{h}) \\ &= \min_{(\mathbf{Q}, \mathbf{h}) \in \Omega^N \times \mathbb{R}^N_{h_{\min}}} \min_{\mathcal{R} = \{\mathcal{R}_n\} \subset \Omega} \bar{P}(\mathbf{Q}, \mathbf{h}, \mathcal{R}).\end{aligned} \tag{21}$$

Like the traditional *$N-$facility locational-parameter optimization problem*[2] in [39], where $\kappa = 0$ and $h_n = 0$, the optimization problem in (21) is a constrained non-convex optimization problem. The computational complexity of finding the global optimum for such an $N-$facility problem has been proved to be NP-hard [41]. To find the local extrema of (19) analytically, we need the objective function $\bar{P}$ to be continuously differentiable at any point in $\Omega^N \times \mathbb{R}_0^N$. Such a property was shown to be true for piecewise continuous

[2]The traditional $N-$facility locational-parameter optimization problem has been widely explored for 2-D deployment and can be solved by Lloyd Algorithm with super-polynomial complexity [40].

non-decreasing cost functions with Euclidean metrics over Ω^N [39, Thm. 2.2] and weighted Euclidean metrics [27]. Then, the necessary condition for a local extremum is the vanishing of the gradient at a critical point[3]. By [27], the gradient of this kind of optimization problem depends on the Voronoi region's geometric characteristics. Thus, in the next lemma, we derive and explore the generalized Voronoi regions for sets $\Omega \subset \mathbb{R}^d$ with $d = 1, 2$ and for any height $h_n \in \mathbb{R}_0$. The derived generalized Voronoi regions are special cases of *Möbius diagrams (tessellations)*, introduced in [26].

Lemma 1. *Let $\mathbf{Q} = (\mathbf{q}_1, \mathbf{q}_2, \ldots, \mathbf{q}_N) \in \Omega^N \subset (\mathbb{R}^d)^N$ for $d \in \{1, 2\}$ be the ground positions and $\mathbf{h} \in \mathbb{R}_+^N$ the associated heights. For fixed parameters $\kappa \geq 1$ and $\gamma \geq \frac{1+\kappa}{2}$ with uniform density λ in Ω, the minimal average power over all possible N regions is given by*

$$\bar{P}\left(\mathbf{Q}, \mathbf{h}\right) = \sum_{n=1}^{N} \int_{\mathcal{V}_n} \frac{\left(\left\|\mathbf{q}_n - \boldsymbol{\omega}\right\|^2 + h_n^2\right)^{\gamma}}{h_n^{\kappa}} \lambda(\boldsymbol{\omega}) d\boldsymbol{\omega}, \tag{22}$$

where the generalized Voronoi region $\mathcal{V}_n = \mathcal{V}_n(\mathbf{Q}, \mathbf{h}) = \bigcap_{m \neq n} \mathcal{V}_{nm}$ and the dominance region of n over m is defined by

$$\mathcal{V}_{nm} = \begin{cases} \{\boldsymbol{\omega} \in \Omega \mid \left\|\mathbf{q}_n - \boldsymbol{\omega}\right\| \leq \left\|\mathbf{q}_m - \boldsymbol{\omega}\right\|\} & , h_m = h_n, \\ \{\boldsymbol{\omega} \in \Omega \mid \left\|\boldsymbol{\omega} - \mathbf{c}_{nm}\right\| \leq r_{nm}\} & , h_n < h_m, \\ \{\boldsymbol{\omega} \in \Omega \mid \left\|\boldsymbol{\omega} - \mathbf{c}_{nm}\right\| \geq r_{nm}\} & , h_n > h_m, \end{cases} \tag{23}$$

where center $\mathbf{c}_{nm}$ and radius r_{nm} of the circle are given by

$$\mathbf{c}_{nm} = \frac{\mathbf{q}_n - h_{nm}\mathbf{q}_m}{1 - h_{nm}} \quad \text{and}$$
$$r_{nm} = \left(\frac{h_{nm}}{\left(1 - h_{nm}\right)^2} \left\|\mathbf{q}_n - \mathbf{q}_m\right\|^2 + h_n^2 \frac{h_{nm}^{1-\frac{2\gamma}{\kappa}} - 1}{1 - h_{nm}} \right)^{\frac{1}{2}}. \tag{24}$$

Here, we denoted the height ratio of the nth and mth UAV by $h_{nm} = \left(h_n / h_m\right)^{\frac{\kappa}{\gamma}}$.

Proof. See Appendix A. ∎

Remark. It is also possible that two UAV ground positions are the same, but have different heights. If the height ratio is very small or very large, one of the UAVs can become redundant, i.e., its region is empty and the UAV is not connected to any UE, as shown in the following example. In fact, optimizing over all UAVs excludes such a case. We showed this fact for the optimal 2-D deployment in [42, Lem. 3].

Example. Fig. 1 plots the UE regions for a uniform distribution in $\Omega = [0, 10]^2$ and $N = 2$ UAVs placed on $\mathbf{q}_1 = (1, 2)$, $h_1 = 4$ and $\mathbf{q}_2 = (6, 6)$, $h_2 = 8$, with parameters $\kappa = 1$ and $\alpha = 2$. If the second UAV reaches an altitude of $h_2 \geq 18.4$, its Voronoi region $\mathcal{V}_2 = \mathcal{V}_{2,1}$ is empty.

A. Necessary optimal conditions

To find the optimal deployment of N UAVs, we have to minimize the average transmit power (18) over all possible UAV positions with minimum flight height h_{min}, i.e., we have to solve the following non-convex *$N-$facility locational-parameter optimization problem* (25) where $\mathcal{V}_n(\mathbf{Q}, \mathbf{h})$ is the Möbius region defined in (23) for a fixed $(\mathbf{Q}, \mathbf{h})$. The integral kernel $f(\left\|\mathbf{q}_n - \boldsymbol{\omega}\right\|^2, h_n) = (\left\|\mathbf{q}_n - \boldsymbol{\omega}\right\|^2 + h_n^2)^{\gamma} / h_n^{\kappa}$ is a non-decreasing positive function in the Euclidean distance of $\mathbf{q}_n$ and $\boldsymbol{\omega}$ for fixed h_n, since $\gamma \geq (1+\kappa)/2 \geq 1$. A point $(\mathbf{Q}^*, \mathbf{h}^*)$ with Möbius diagram $\mathcal{V}^* = \mathcal{V}(\mathbf{Q}^*, \mathbf{h}^*) = \{\mathcal{V}_1^*, \ldots, \mathcal{V}_N^*\}$ is a critical point of (25) if all horizontal partial derivatives of $\bar{P}$ and the vertical partial derivatives of $\bar{P}$ are vanishing , i.e., if for each $n \in [N]$, we have (26) and (27) [27]. If $h_n^* < h_{\min}$, then we set $h_n^* = h_{\min}$. In this case, the global optimal deployment is not admissible and $(\mathbf{Q}^*, \mathbf{h}^*)$ becomes a local optimum. However, it is possible to achieve a global optimum, by adjusting the parameters α, κ, N, and Ω accordingly. For $N = 1$, the integral regions do not depend on $\mathbf{Q}$ or $\mathbf{h}$ and since the integral kernel f is continuously differentiable and non-decreasing in $\left\|\mathbf{q}_n - \boldsymbol{\omega}\right\|^2$, the partial derivatives only apply to the integral kernel [43]. For $N > 1$, the conservation-of-mass law [39] can be used to show that the derivatives of the integral domains cancel each other, see [27] for a detailed proof.

Remark. The shape of the regions depends on the UAV heights. If the height is different for each UAV (heterogeneous), some region boundaries will be spherical instead of polyhedral. Later, we show that homogeneous (common) heights with polyhedral regions are optimal.

B. Optimal common height in a 3-D UAV deployment

We showed in the conference paper version of this work [1] that, in an optimal 2-D deployment, UAVs settle at a common flight height in the asymptotic limit ($N \to \infty$). Therefore, let us assume a common height for all UAVs in the 3-D deployment. By simulations, we show in Section V that the optimal deployment indeed converges to a common height deployment for large N. For any common height, Lemma 1 shows that the ground regions are polyhedral, since the cost function is homogeneous. Hence, in the asymptotic limit, the optimal ground positions result in congruent hexagonal regions given a fixed common height [43].

In fact, we can show that the 3-D UAV deployment problem with a common height restriction and for large N has only one local optimum deployment, given by centroidal ground positions with hexagonal regions and an optimal common height h^*.

Theorem 1. *Let $\kappa \geq 1, \gamma \geq (1 + \kappa)/2$, and $\Omega \subset \mathbb{R}^2$ be a set with area $\mu(\Omega) = A > 0$. For a uniform density λ over Ω, the optimal deployment of N UAVs, minimizing the average transmit-power in (25) under the restriction of a common height, with ground locations $\mathbf{Q}^* = (\mathbf{q}_1^*, \ldots, \mathbf{q}_N^*)$ and common height h^* is attained asymptotically ($N \to \infty$, high resolution case) by the hexagonal lattice, where each Voronoi region $\mathcal{V}_n^*$ is congruent to the hexagon $\mathcal{H}$ and the optimal ground locations are the corresponding centroids. Moreover, the global optimal common height is given by $h^* = h^*(\gamma, \kappa, H)$ for $H = A/N$. For $\gamma = 1, 2, 3$, we derive the optimal height asymptotically as*

[3] If $\nabla \bar{P}$ is not continuous in $\mathcal{P}^N$, then any jump-point is a potential critical point and has to be checked individually.

$$\bar{P}(\mathbf{Q}^*,\mathbf{h}^*)=\min_{\mathbf{Q}\in\Omega^N,\mathbf{h}\in\mathbb{R}^N_{h_{\min}}}\sum_{n=1}^{N}\int_{\mathcal{V}_n(\mathbf{Q},\mathbf{h})}h_n^{-\kappa}(\|\mathbf{q}_n-\boldsymbol{\omega}\|^2+h_n^2)^{\gamma}\lambda(\boldsymbol{\omega})d\boldsymbol{\omega}, \tag{25}$$

$$\nabla_{\mathbf{q}_n}\bar{P}\Big|_{\mathbf{q}_n=\mathbf{q}_n^*}=\frac{2\gamma}{h_n^{*\kappa}}\int_{\mathcal{V}_n^*}(\mathbf{q}_n^*-\boldsymbol{\omega})(\|\mathbf{q}_n^*-\boldsymbol{\omega}\|^2+h_n^{*2})^{\gamma-1}\lambda(\boldsymbol{\omega})d\boldsymbol{\omega}=\mathbf{0}, \tag{26}$$

$$\nabla_{h_n}\bar{P}\Big|_{h_n=h_n^*}=\frac{\kappa}{h_n^{*\kappa+1}}\int_{\mathcal{V}_n^*}\left(\frac{2\gamma h_n^{*2}}{\kappa}(\|\mathbf{q}_n^*-\boldsymbol{\omega}\|^2+h_n^{*2})^{\gamma-1}-(\|\mathbf{q}_n^*-\boldsymbol{\omega}\|^2+h_n^{*2})^{\gamma}\right)\lambda(\boldsymbol{\omega})d\boldsymbol{\omega}=0. \tag{27}$$

$$h^*(\gamma,\kappa,H)\sim c(\gamma,\kappa)\sqrt{H}\quad for\quad 1\le\kappa\le 2\gamma-1, \tag{28}$$

with scaling factors (29)*, where*

$$u(\kappa)=(143360-16728\kappa-444\kappa^2+37\kappa^3)/4375, \tag{30}$$

$$v(\kappa)=\frac{12(6-\kappa)}{125\cdot 35}\sqrt{\frac{3}{5}}\cdot \sqrt{6607552+659680\kappa+103387\kappa^2-108408\kappa^3+9034\kappa^4}, \tag{31}$$

which achieves for $\beta_0=1$ *and directivity* $D_0(\kappa)$ *in* (6) *the minimal average transmit powers* (32)*.*

Proof. See Appendix B ∎

Remark. The optimal common height in (28) scales with $c(\gamma,\kappa)$, which increases with κ for fixed γ. Note that $c(\gamma,\kappa)\le 1$ for $\gamma\in\{1,2,3\}$ and all admissible $1\le\kappa\le 2\gamma-1$. For a realistic path-loss model of the wireless link in (2), the ratio $H=A/N$ and the parameters α and κ have to be chosen such that the optimal height satisfies $h^*\ge h_{\min}>d_0\ge 1$, where $h_{\min}$ is the minimum height constraint. Combining $c(\gamma,\kappa)\le 1$ and (28) results in $H>1$. In the asymptotic limit, $H=A/N$ can be seen as the *cell (region) size* per UAV, i.e., the size of the hexagon $\mathcal{H}$. Note that if $d_0=1$, then β_0 in (13) is independent of α.

Although, the analytic results in Theorem 1 are only asymptotic in N, simulations in Section V validate similar results already for $N=100$ UAVs. Hence, deploying the N UAV ground positions on a hexagonal grid at a common height (28), yields a very power-efficient uplink coverage of the UEs. Due to the non-linearity of the problem, the closed-form solutions of the height (28) and power (32) are difficult to derive. However, using the proof techniques in Appendix B, the optimal common height $h^*=\sqrt{z^*}$ for any α,γ combinations can be calculated numerically by solving (40) for z. Using hexagonal Voronoi regions and inserting the optimal common height in (25) results in the minimal average transmit-power of the UEs. Therefore, the closed-form solutions in Theorem 1 can be used to study the general behavior of the optimal deployment, such as the optimal power behavior over cell size H or beamwidth (antenna) parameter κ, as shown in Fig. 3. Here, Fig. 3a and Fig. 3b show the minimum average transmit-power in dB over H for $\kappa=1$ and over various $1\le\kappa\le 2\gamma-1$ and $\gamma=1,2,3$ corresponding to $\alpha=2\gamma-\kappa$, respectively. Note that, in Fig. 3b, an increase in κ decreases α since γ is fixed. Since the directivity $D_0=2(\kappa+1)$ increases with κ, it reduces the average transmit-power in (32). For $\alpha=1$ and $\kappa=1$ (solid curve), we gain 3 dB if we use $\kappa=3$ (dashed curve). Hence, in Fig. 3b, $\bar{P}^*(2,3,100)$ is the smallest average transmit power for $H=100$, given for example by $N=100$ UAVs covering $\Omega=[0,100]^2$.

Moreover, it can be seen that the (local) optimal heights (28) scale with $\sqrt{H}$ and the transmit-powers (32) scale with $(\sqrt{H})^{2\gamma-1}$, since the power depends on the height in (51) by a power of maximal $2\gamma-1$. Indeed, the derivations for $\gamma=1,2,3$ show a power scaling with $H^{\gamma-1/2}$. Hence, for large H and constant κ, the average power $\bar{P}^*$ increases in $\gamma\ge 1$, as can be seen in Fig. 3a. On the other hand, for fixed κ, $c(\gamma,\kappa)$ decreases in $\gamma\ge 1$ and so the common optimal height. We can also confirm this behavior by simulations in Fig. 8a for fixed $\kappa\in\{1,2\}$ and H. Similar results hold for the 2-D deployment and can be shown analytically [42, Thm. 1].

Let us note that, in the high-resolution case, all values of cell size $H=A/N$ can be achieved by an appropriate choice of the target size A. An increase of κ for fixed α can change the transmit-power, but only slightly changes the optimal common height. Hence, the optimal κ can be determined to minimize the transmit-power by optimizing the effective beamwidth.

From simulations in the next section, for a uniform user density, we see that restricting the heights to be the same, i.e., a common height, does not lead to larger average transmit-power if N is very large. Therefore, we conjecture that the optimal common height with centroidal ground positions asymptotically achieves the global minimum average transmit-power.

IV. Llyod-like Algorithms

In this section, we introduce two Lloyd-like algorithms, presented in Algorithm 1, to optimize the deployment for 3-D scenarios. The proposed algorithms iterate between two steps: (i) The partitioning is optimized while the UAV positions are fixed; (ii) The UAV positions are optimized through gradient descent while the ground cell partitioning is fixed. In Lloyd-A, all UAVs share a common height while Lloyd-B allows UAVs with different heights. Like Lloyd Algorithm, Lloyd-A and Lloyd-B are iterative improvement algorithms and converge. In Section III, we have proved that generalized Voronoi regions are the optimal cell partitions for a given UAV deployment. Therefore, the average power cannot increase in Step (i). During Step (ii), the cell partition is fixed and the original optimization problem can be divided into N separate subproblems: $\min_{(\mathbf{q}_n,h_n)\in\Omega\times\mathbb{R}_{h_{\min}}}\int_{\mathcal{V}_n}\frac{(\|\mathbf{q}_n-\boldsymbol{\omega}\|^2+h_n^2)^{\gamma}}{h_n^{\kappa}}\lambda(\boldsymbol{\omega})d\boldsymbol{\omega}$, for all $n\in\{1,\dots,N\}$. Each UAV attempts to move along the opposite direction of the gradient to reduce the power over its own cell partition $\mathcal{V}_n$. To avoid power increase, a complete loop over n is applied to tune the movement distance. As a result, each UAV will stay still or move to a new location with smaller power consumption. Thus, Step (ii) cannot increase

$$c(1)=\sqrt{\frac{5}{18\sqrt{3}}},\ c(2,\kappa)=\sqrt{\frac{5}{18\sqrt{3}}\frac{\sqrt{(172-43\kappa)\frac{\kappa}{125}+4}-(2-\kappa)}{4-\kappa}},\ c(3,\kappa)=\sqrt{\frac{5}{18\sqrt{3}}\frac{(u(\kappa)-v(\kappa))^{\frac{1}{3}}+(u(\kappa)+v(\kappa))^{\frac{1}{3}}-(4-k)}{6-\kappa}} \quad (29)$$

$$\bar{P}^*(1,1,H)\sim\frac{1}{D_0(1)}\sqrt{\frac{10}{9\sqrt{3}}}H^{\frac{1}{2}},\quad \bar{P}^*(2,\kappa,H)\sim\frac{1}{D_0(\kappa)}\left(\frac{14}{405c(2,\kappa)}+\frac{5c(2,\kappa)}{9\sqrt{3}}+c^3(2,\kappa)\right)H^{\frac{3}{2}},$$

$$\bar{P}^*(3,\kappa,H)\sim\frac{1}{D_0(\kappa)}\left(\frac{83}{195\cdot 27c(3,\kappa)}+\frac{14c(3,\kappa)}{135}+\frac{5c^3(3,\kappa)}{9\sqrt{3}}+c^5(3,\kappa)\right)H^{\frac{5}{2}}. \quad (32)$$

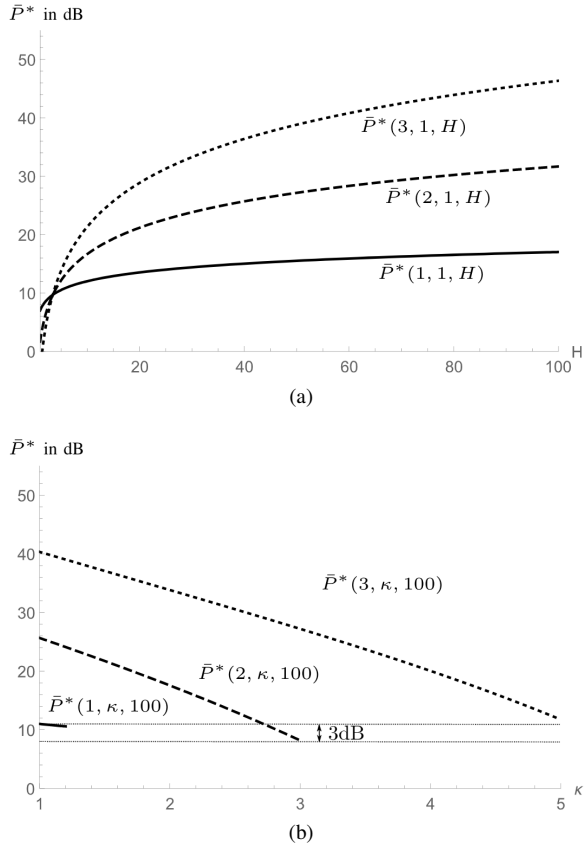

Fig. 3: Optimal average-powers for $\gamma=1,2,3$ (a) over cells of size $H=A/N$ for $\kappa=1$ and (b) over various κ for $H=100$.

the power consumption either. In addition, we limit UAVs' vertical movement to satisfy the constraint $h_n \geq h_{\min}$. The main difference between Lloyd-A and Lloyd-B is in the computation of the gradients. The gradient formula for Lloyd-B is provided by Eqs. (26) and (27). To derive the same formula for Lloyd-A, the N heights, $\{h_n\}$, are replaced by a common height h. Then, the partial derivative with respect to h is the sum of the partial derivatives with respect to h_n, i.e., $\nabla_h=\sum_{n=1}^{N}\nabla_{h_n}|_{h_n=h}$.

A. Algorithm Complexity

Before calculating the complexity of Lloyd-A and Lloyd-B algorithms, we need to study the complexity of computing gradient $\{\nabla_{\mathbf{q}_n},\nabla_{\mathbf{h}_n}\}$ and generalized Voronoi regions $\{\mathcal{V}_n\}$. Both $\nabla_{\mathbf{q}_n}$ and $\nabla_{\mathbf{h}_n}$ are integrals over generalized Voronoi region $\mathcal{V}_n$. Many methods to calculate integrals, such as uniform sampling, stratified sampling, importance sampling, sequential Monte Carlo, and Risch algorithm are available in the literature [44], [45]. For simplicity, we assume the integrals in $\nabla_{\mathbf{q}_n}$ and $\nabla_{\mathbf{h}_n}$ are calculated by uniform sampling[4]. In this case, the computational complexity of $\nabla_{\mathbf{q}_n}$ and $\nabla_{\mathbf{h}_n}$ is proportional to the number of samples, $O(\frac{\mu(\mathcal{V}_n)}{\tau})$, where τ is the sample size. Thus, the total complexity of computing all $\nabla_{\mathbf{q}_n}$ and $\nabla_{\mathbf{h}_n}$ terms is $O(\frac{\sum_{n=1}^{N}\mu(\mathcal{V}_n)}{\tau})=O(\frac{\mu(\Omega)}{\tau})$. Similarly, the total power $\bar{P}(\mathbf{Q}^*,\mathbf{h}^*)$ is an integral over Ω and can be

Algorithm 1 Lloyd-like Algorithms (Lloyd-A and Lloyd-B)

Input: Target area: Ω; probability density function: $\lambda(\cdot)$; the initial UAV ground deployment: $\mathbf{Q}=(\mathbf{q}_1,\mathbf{q}_2,\ldots,\mathbf{q}_N)$; the initial UAV heights: $\mathbf{h}=(h_1,h_2,\ldots,h_N)$ ($h_1=h_2=\cdots=h_N$ for Lloyd-A); path-loss exponent: α; the antenna pattern exponent: κ; the minimum flight height: h_{min}; the initial step size: δ; the stop threshold: ϵ; the maximum number of iterations for the external loop: L_{ex}; the maximum number of iterations for the internal loop: L_{in}.

Output: the final UAV ground deployments $\mathbf{Q}=(\mathbf{q}_1,\mathbf{q}_2,\ldots,\mathbf{q}_N)$; the final flight height: $\mathbf{h}=(h,\ldots,h)$ for Lloyd-A or $\mathbf{h}=(h_1,h_2,\ldots,h_N)$ for Lloyd-B; Total average transmit-power at the final deployment $\bar{P}(\mathbf{Q},\mathbf{h})$.

Calculate the generalized Voronoi regions $\{\mathcal{V}_n\}_{n\in\{1,\ldots,N\}}$.
Initialize the external loop index $i=1$
do
  Calculate the old total power $\bar{P}_{old}=\bar{P}(\mathbf{Q},\mathbf{h})$
  Calculate the gradient $\nabla_{\mathbf{q}_n}$ and $\nabla_{\mathbf{h}_n}$ by (26) and (27)
  Initialize step size $t=\delta$
  if ($\nabla_{\mathbf{q}_n}\neq 0$ or $\nabla_{\mathbf{h}_n}\neq 0,\ \forall\, n\in\{1,\ldots,N\}$) **then**
    do
      Initialize the internal loop index $j=1$
      Calculate the ground positions $\mathbf{q}'_n=\mathbf{q}_n-t*\nabla_{\mathbf{q}_n}$
      Calculate the new UAV flight heights $\begin{cases} h'_n=\max(h_{\min},h_n-t*\sum_n\nabla_{\mathbf{h}_n}), & \text{Lloyd-A}\\ h'_n=\max(h_{\min},h_n-t*\nabla_{\mathbf{h}_n}), & \text{Lloyd-B}\end{cases}$
      Adjust the step size $t=t/2$
      Calculate the power $\bar{P}(\mathbf{Q}',\mathbf{h}')$
    while $\bar{P}(\mathbf{Q},\mathbf{h})\leq\bar{P}(\mathbf{Q}',\mathbf{h}')$ and $j<L_{in}$
  end if
  Update UAV deployment $\mathbf{Q}=\mathbf{Q}'$, $\mathbf{h}=\mathbf{h}'$
  Update the generalized Voronoi regions $\{\mathcal{V}_n\}_{n\in\{1,\ldots,N\}}$.
  Calculate the new total power $\bar{P}_{new}=\bar{P}(\mathbf{Q},\mathbf{h})$
  $i=i+1$
while $\frac{\bar{P}_{old}-\bar{P}_{new}}{\bar{P}_{old}}>\epsilon$ and $i<L_{ex}$

[4]The integral is approximated by the summation over uniform samples.

calculated within $O(\frac{\mu(\Omega)}{\tau})$.

Next, we analyze the computational complexity of generalized Voronoi regions. Since all UAVs share a common height in Lloyd-A, the 2-D generalized Voronoi regions are degraded to standard 2-D Voronoi regions and can be computed with complexity $O(N)$ [46]. For Lloyd-B, we use a 2-D generalized Voronoi diagram which has the same structure as the 2-D multiplicatively weighted Voronoi diagram[5]. As a result, the 2-D generalized Voronoi diagram and the 2-D multiplicatively weighted Voronoi diagram have the same complexity $O(N^2)$ [47].

Now, we use the above analysis to derive the complexity of the proposed algorithms. Given $\nabla_{\mathbf{q}_n}$ and $\nabla_{\mathbf{h}_n}$, the computational complexity of $\mathbf{q}'_n$ and h'_n is O(1) while calculating the power $\bar{P}(\mathbf{Q}', \mathbf{h}')$ has complexity $O\left(\frac{\mu(\Omega)}{\tau}\right)$. Thus, the complexity of the internal loop (Lines 8 - 14) can be determined as $O\left(L_{in}\left(O(\frac{\mu(\Omega)}{\tau}) + O(1)\right)\right) = O\left(\frac{L_{in}\mu(\Omega)}{\tau}\right)$, where L_{in} is the maximum number of iterations of the internal loop. In the external loop, we calculate the gradient and cell partitioning. Therefore, the total complexity for Lloyd-A is $O\left(L_{ex} \cdot O(\frac{L_{in}\mu(\Omega)}{\tau}) + O(\frac{\mu(\Omega)}{\tau}) + N\right) = O\left(L_{ex}\left(\frac{L_{in}\mu(\Omega)}{\tau} + N\right)\right)$, where L_{ex} is the maximum number of iterations of the external loop. Similarly, the complexity of Loyd-B is $O\left(L_{ex}\left(\frac{L_{in}\mu(\Omega)}{\tau} + N^2\right)\right)$.

V. Simulation Results

In what follows, we provide simulation results over the 2-D target region $\Omega = [0, 1000]^2$ with uniform and non-uniform density functions. The non-uniform density function is a Gaussian mixture of the form $\frac{\sum_{k=1}^{3} \frac{A_k}{\sqrt{2\pi\sigma_k^2}} \exp\left(-\frac{\|\boldsymbol{\omega}-\mathbf{c}_k\|^2}{2\sigma_k}\right)}{\int_\Omega \left(\sum_{k=1}^{3} \frac{A_k}{\sqrt{2\pi\sigma_k^2}} \exp\left(-\frac{\|\boldsymbol{\omega}-\mathbf{c}_k\|^2}{2\sigma_k}\right)\right) d\omega}$, where the weights, A_k, $k = 1, 2, 3$ are 0.5, 0.25, 0.25, the means, $\mathbf{c}_k$, are $(300, 300)$, $(600, 700)$, $(750, 250)$, the standard deviations, σ_k, are 1.5, 2, and 1, respectively. All length parameters are measured in meters. The power values depend on the fixed parameters defining β_0 in (13), given by the bandwidth B, data-rate R_b, noise-power N_0 at the UAV, channel attenuation power σ_ψ^2, antenna characteristic K, UE antenna gain G_{TX} ($= 1$ for perfect isotropic antennas), and the reference distance d_0^α (usually set to 1). The beam-exponent κ_{LoS} and path-loss exponent α are dimensionless and can be adjusted to obtain optimal heights and average-transmit powers in a desired range. In our simulations, we set $\beta_0(2) = 10^{-2}$ m^2/W, $\beta_0(3) = 10^{-3}$ m^3/W, and $\beta_0(4) = 10^{-4}$ m^4/W.

To evaluate the performance, we compare the average transmit-power in Watt for deployments derived by Lloyd-A, Lloyd-B, the algorithm in [18], denoted by KSS, and the algorithm in [13], denoted by MSBD, with various path-loss exponents α and various minimum heights[6]. KSS deployment Algorithm is designed to minimize the average power of UAVs with omni-directional antennas whose antenna gains are identical among all directions ($\kappa_{\text{LoS}} = 0$). Taking a "constant" directional antenna pattern into consideration, MSBD Algorithm applies a circle packing [48] to derive the ground positions of the N UAVs with a common cell radius[7] and then determines the heights in terms of θ_{HPBW}. In our simulations, the HPBW for "constant" antenna patterns is set to $\theta_{\text{HPBW}} = 120°$. To make a fair comparison, the directivity parameter for cosine-shape patterns is set to $\kappa_{\text{LoS}} = 1$, which according to (8) corresponds to $\theta_{\text{HPBW}}(1) = 120°$. For $\kappa_{\text{LoS}} = 2$, we obtain $\theta_{\text{HPBW}}(2) = 90°$. Lloyd-like algorithms (KSS, Lloyd-A and Lloyd-B) require an initial UAV deployment. We generate 100 initial UAV deployments randomly, i.e., every UAV location is generated according to a uniform distribution on $1000 \times 1000 \times 100$. Then, the Lloyd-like algorithms are initialized with the generated random deployments and the power is calculated as the average over 100 runs.

The performance comparisons for different path-loss parameters and different minimum heights are shown in Fig. 4. The omni-antenna power and cosine-directional-antenna power are calculated from (18) divided by the maximum directivity[8] (6) with $\kappa_{\text{LoS}} = 0$ and $\kappa_{\text{LoS}} = 1$, respectively. Note that KSS Algorithm generates the optimal deployment for UAVs with omni-antennas. When the number of UAVs is large, Fig. 4 shows that KSS Algorithm can benefit from replacing omni-antennas by cosine-directional antennas. However, when the number of UAVs is small, KSS Algorithm spends more energy on cosine-directional antennas compared to omni-antennas. For example, given 20 UAVs in Fig. 4a, KSS Algorithm spends the average power of $\bar{P} = 0.98$ (W) on cosine-directional antennas which is larger than that of omni-antennas, i.e., $\bar{P} = 0.91$ (W). However, if 40 UAVs are deployed, the omni-antenna power $\bar{P} = 0.48$ (W) exceeds the cosine-directional antenna power of $\bar{P} = 0.37$ (W). Moreover, one can save power by deploying more UAVs or using an environment with less path-loss exponent. On one hand, deploying more UAVs will reduce the overall communication distance between UEs and UAVs and thus spend less power. On the other hand, a small path-loss exponent α means less power attenuation. Thus, given the communication distance, the environment with a small α is more energy efficient.

By comparing the average powers of cosine-directional-antennas provided by different algorithms, we can conclude that the proposed Lloyd-B is the best solution for cosine-directional-antennas. Moreover, cosine-directional-antennas' minimum powers which are achieved by Lloyd-B, are always smaller than omni-antennas' minimum powers which are achieved by KSS Algorithm. In other words, cosine-directional-antennas are more energy-efficient compared to omni-antennas. An intuitive explanation is that omni-antennas radiate power among all directions, which is a waste of energy, while cosine-directional-antennas concentrate the power to a specific UE cell on the ground. Furthermore, using cosine-directional-antennas, UAVs can cover all UEs in the target area

[5]The only difference between the generalized Voronoi diagram and multiplicatively weighted Voronoi diagram is the value of the centroid and radii which are provided in Eq. (24).

[6]To make KSS and MSBD Algorithms satisfy the minimum height constraint, we adjust their final heights by $h_{\min}$, i.e., $h_n = \max(h_n, h_{\min})$.

[7]The optimal $N-$circle packing over a square can be found, e.g., at http://hydra.nat.uni-magdeburg.de/packing/csq/csq.html.

[8]In Section II, we assume $\beta_0(\alpha)D_0(\kappa_{\text{LoS}}) = 1$ for simplicity. However, when we compare the powers of different antennas (or different κ_{LoS}s), the antenna directivity $D_0(\kappa_{\text{LoS}})$ is taken into account.

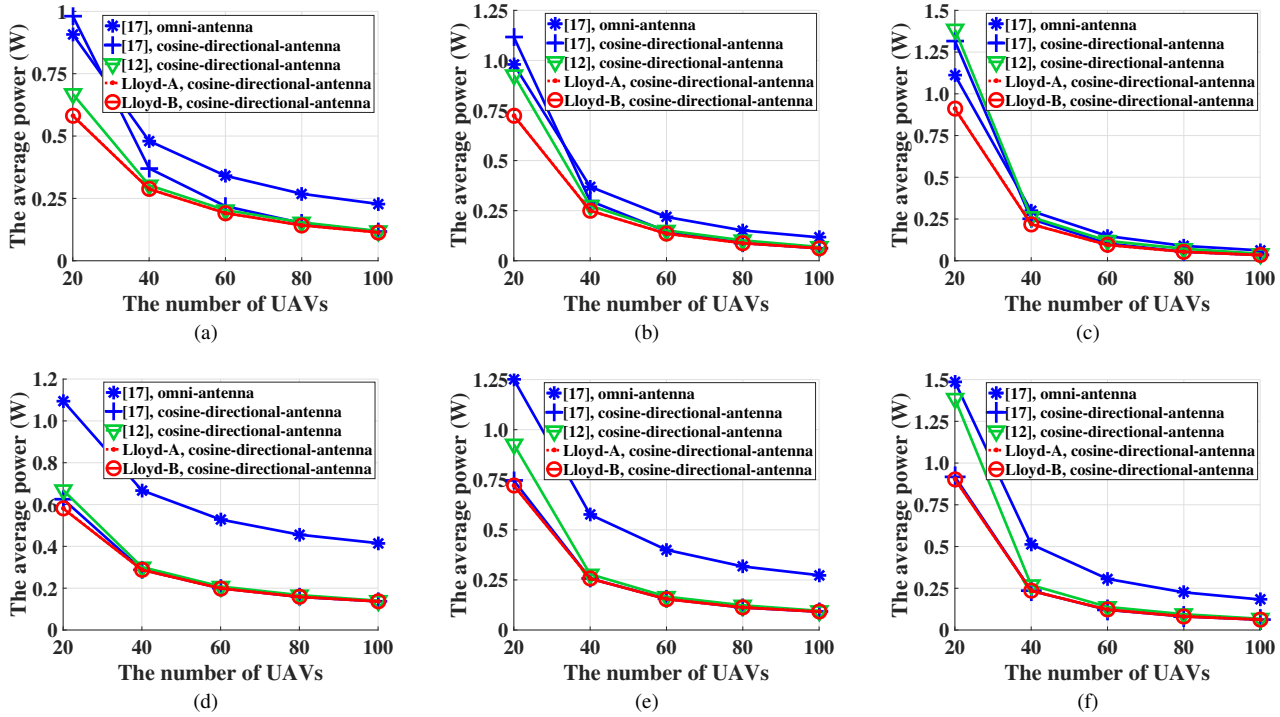

Fig. 4: The performance comparison for various path-loss exponents α and various minimum heights with the uniform density function and beam-exponent $\kappa_{\text{LoS}} = 1$ and NLoS exponent $\kappa_{\text{NLoS}} = 0$. (a) $\alpha = 2$, $h_{\min} = 25$; (b) $\alpha = 3$, $h_{\min} = 25$; (c) $\alpha = 4$, $h_{\min} = 25$; (d) $\alpha = 2$, $h_{\min} = 50$; (e) $\alpha = 3$, $h_{\min} = 50$; (f) $\alpha = 4$, $h_{\min} = 50$.

while MSBD Algorithm using a constant-directional antenna model achieves only a partial coverage, due to non-overlapping circular ground cells. For example, if we apply constant-directional-antenna pattern to MSBD deployment in Fig. 4a, the coverage will be dropped from 100% to 78.54%. In fact, the constant-directional-antenna model is an ideal but not realistic antenna model. Thus, one should use model (5) rather than model (1) to evaluate the power consumption. The gap between the green and red curves in Figs. 4 and 5 shows how much power we can save by using our proposed deployment against MSBD deployment with the realistic model (5). For a given deployment, when the constant-directional-antenna model is replaced by the realistic cosine-directional-antenna model, the corresponding power is significantly increased. Furthermore, the circle packing solution, used in MSBD Algorithm, is only available over some special-shaped target regions, e.g, squares and circles. However, Lloyd-A(B) can be applied to arbitrary target regions.

From Fig. 4, one can also find that the average powers spent by Lloyd-A and Lloyd-B are very close (the difference is less than 0.5%), indicating the optimality of the common height when the density function is uniform. However, the gap between Lloyd-A and Lloyd-B in Figs. 5a, 5b, 5c for a non-uniform density function is non-negligible. For instance, given 20 UAVs with path-loss exponent $\alpha = 3$, the average power by Lloyd-A is 0.56 (W) while the average power by Lloyd-B is only 0.52 (W) which is 7.1% lower. As a result, the optimality of the common height cannot be extended to the scenarios with non-uniform density functions. Intuitively, the system should allocate more resources, e.g., UAVs, to the high density region. As a result, the cell size in a high density region should be smaller than that of a low density region. As we will see in Section V-A, UAVs tend to have lower heights with smaller cell sizes. Therefore, instead of flying on a common height, UAVs over a non-uniform distributed target region will have relatively low altitudes in high density regions and relatively high altitudes in low density regions. Meanwhile, the minimum flight height has an influence on the deployment. If the minimum flight height is large, it may limit the capability of the algorithm to choose the best locations and force it to place the UAVs at the minimum height. For example, Lloyd-A(B), like KSS Algorithm, places UAVs at the height of 50 in Figs. 4d, 4e and 4f. As a result, the average power of KSS Algorithm with cosine-directional-antennas is much closer to that of Lloyd-A(B) in Figs. 4d, 4e and 4f. Nonetheless, as shown in Figs. 4d, 4e, and 4f, Lloyd-A(B)'s power is not larger than that of KSS Algorithm even if the performance is limited by a large minimum flight height.

To study the influence of beamwidth which is reflected by κ_{LoS}, we compare the average power for various κ_{LoS}s. Fig. 6a shows that the minimum power for different $h_{\min}$s is achieved by different beamwidths. When the height constraint is loose[9], i.e., $h_{\min} = 25$, the power increases as the κ_{LoS} goes up and the minimum power is achieved at $\kappa_{\text{LoS}} = 1$. When $h_{\min}$ is increased to 50 m, optimal UAV heights with small beamwidth are limited to 50 m. In this case, the minimum power for uniform and non-uniform distributions is achieved at $\kappa_{\text{LoS}} = 2.5$ and $\kappa_{\text{LoS}} = 3.5$, respectively. The power decreases as κ_{LoS} increases for a tight constraint, i.e., $h_{\min} = 100$ m, where UAV heights are fixed to 100 m. Consequently, we

[9]Without the constraint on minimum fight, optimal UAV heights for $\kappa \in [1, 4]$ are between 25 m and 75 m.

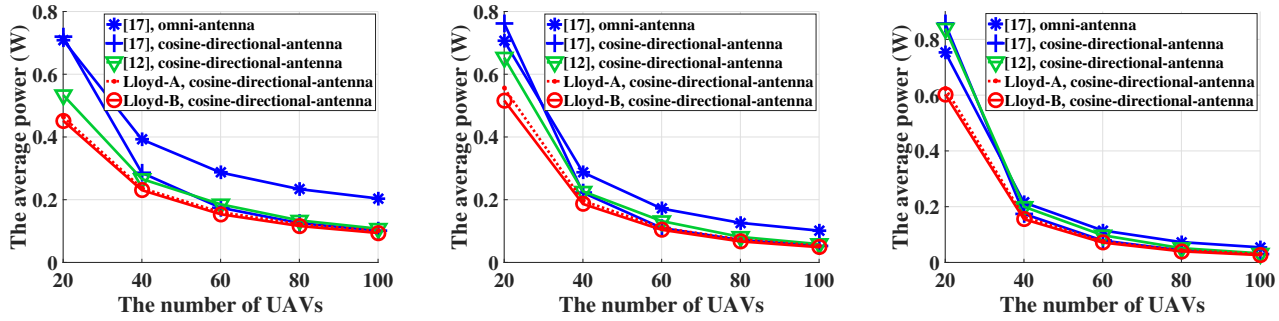

(a) (b) (c)

Fig. 5: The performance comparison for various path-loss exponents α and various minimum flight heights with a non-uniform density function and beam-exponent $\kappa_{\text{LoS}} = 1$ and NLoS exponent $\kappa_{\text{NLoS}} = 0$. (a) $\alpha = 2$, $h_{\min} = 25$; (b) $\alpha = 3$, $h_{\min} = 25$; (c) $\alpha = 4$, $h_{\min} = 25$.

should use broad beamwidth (small κ_{LoS}) for low-altitude UAVs and narrow beamwidth (large κ_{LoS}) for high-altitude UAVs. Furthermore, as we mentioned in Section II, adding NLoS components can be approximated by adding κ_{NLoS} to κ_{LoS} and effectively increasing the cosine power. Form Fig. 6b, we observe that the average power increases as κ_{NLoS} goes up, which means the NLoS component leads to more power consumption.

Figs. 7a and 7b illustrate the UAV ground cells and their partitions for a uniform distribution and square region. As the number of UAVs increases, the UAV partitions converge to hexagons. This implies that the optimality of congruent partitioning in the 1-D case [42, Thm. 1] might be valid for uniformly distributed users in the 2-D case as well. However, the UAV partitions in Figs. 7c and 7d show that congruent partitioning is not optimal for a non-uniform distribution.

A. Different antenna beamwidths

Let us investigate the effect of the beamwidth parameter $\kappa_{\text{LoS}} = \kappa$ on the average power by setting $\kappa_{\text{NLoS}} = 0$, i.e., ignoring the NLoS. If we increase the antenna parameter κ in (5), the radiation gain concentrates on a smaller area and hence decreases the effective beamwidth. This affects the scaling factors $c(\gamma, \kappa)$ and directivity $D_0(\kappa)$ in Theorem 1 but not the dependence on H. To verify the optimal common heights derived in Theorem 1, we first perform a brute force search to obtain the optimal height for one UAV over uniformly distributed regular hexagons with different sizes. For each regular hexagon, we generate 5000 samples [10] and compare the powers. The optimal UAV height is the one with the minimum power among the generated samples. Fig. 8 depicts the optimal common heights of one UAV over a regular hexagon for $\kappa = 1$ and $\kappa = 2$. Overall, the optimal common height increases as the number of UAVs increases. For a constant target area, increasing the number of UAVs, N, results in a finer partition/tessellation/quantization of the target area, i.e., in more cells. Therefore, the cell sizes shrink. As a result, using the same beamwidth, UAVs at a lower height can still provide the full coverage. At the same time, lowering the height results in a smaller path-loss and therefore smaller required average transmit power. Hence, the optimal power efficient solution will have a smaller common height for larger N. Besides, the optimal common height increases if κ increases, but the average power does not necessarily decrease by increasing κ, as is the case in Fig. 3b. Such a conclusion is only valid for large N where $\sqrt{H} \ll h^*$ and the cells are small enough such that small beams can compensate the path-loss by antenna gains.

Moreover, we employ Lloyd-B to get the standard deviation of the optimal heights of multiple UAVs over a uniformly distributed 10×10 square. From Fig. 8b, we find that the standard deviation of heights decreases as the number N of UAVs increases. We also observe the same trend for other κs by simulations. In other words, in the asymptotic regime, the UAVs tend to have approximately an optimal common height[11].

VI. Conclusions

We studied a continuous coverage problem with N UAVs for providing a static reliable wireless communication link to ground users in a given target area. We adopted a realistic angle-dependent directional antenna model for the UAVs and an ideal omni-directional antenna model for the ground users. We derived the exact average power consumption of the users to establish a reliable upload link to the UAVs at a given bandwidth, noise power, and bit-rate. The optimal 3-D deployment of the UAVs for minimizing the average transmit-power of the ground users is derived in closed-form for an arbitrary path-loss exponent, antenna beamwidth, area size, and number of UAVs. Using the derived necessary conditions for optimal deployment, we designed Lloyd-like algorithms to minimize the transmit-power. We demonstrated numerically with brute-force search that asymptotically the global optimal deployment is provided by a hexagonal lattice of the UAV ground positions and a unique common flight height. We derived closed-form solutions for the optimal common height. The optimal common height depends on the cell size per UAV, the antenna beamwidth, and the path-loss exponent. Our deployment algorithm can be used for static or airborne base-stations. An optimal power efficient deployment reduces interference with other wireless communications as well, which again saves power and resources.

[10] 5000 UAV heights are uniformly selected from $[0, L]$, where $L = 2R$ is the length of the regular hexagon. UAV ground position is placed at the geometric centroid of the hexagon according to Theorem 1.

[11] Due to the boundary effect, i.e., the target region cannot be perfectly divided by congruent hexagons and the UAV heights are not exactly the same.

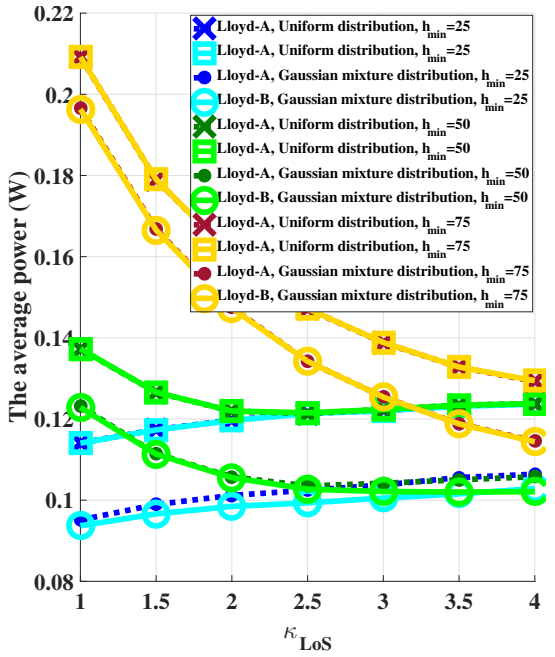

(a)

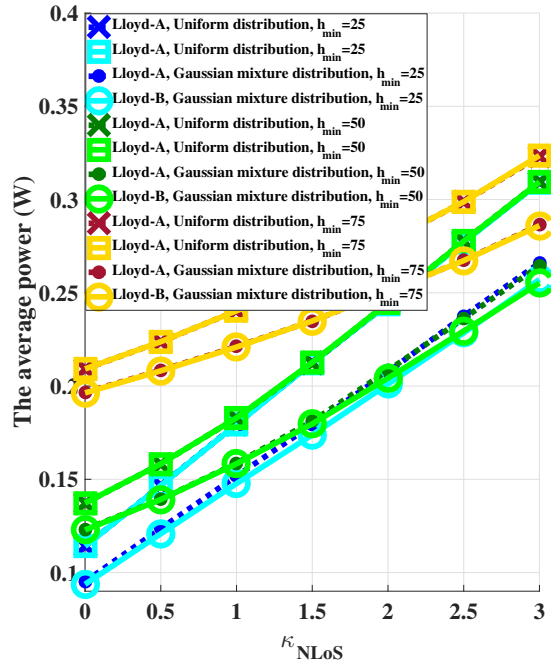

(b)

Fig. 6: The performance comparison with 100 UAVs for various minimum heights $h_{\min}$ and various density function $\lambda(\omega)$. The path-loss exponent is set to $\alpha = 2$. (a) $\kappa_{\text{LoS}} \in [1, 4]$, $\kappa_{\text{NLoS}} = 0$; (b) $\kappa_{\text{LoS}} = 1$, $\kappa_{\text{NLoS}} \in [0, 3]$.

Appendix A
Proof of Lemma 1

The minimization of the distortion functions over Ω defines an assignment rule for a generalized Voronoi tessellation $\mathcal{V}(\mathbf{Q}, \mathbf{h}) = \{\mathcal{V}_1, \mathcal{V}_2, \ldots, \mathcal{V}_N\}$ where

$$\mathcal{V}_n = \mathcal{V}_n(\mathbf{Q}, \mathbf{h}) \tag{33}$$
$$= \{\boldsymbol{\omega} \in \Omega | a_n \left\|\mathbf{q}_n - \boldsymbol{\omega}\right\|^2 + b_n \leq a_m \left\|\mathbf{q}_m - \boldsymbol{\omega}\right\|^2 + b_m, m \neq n\}$$

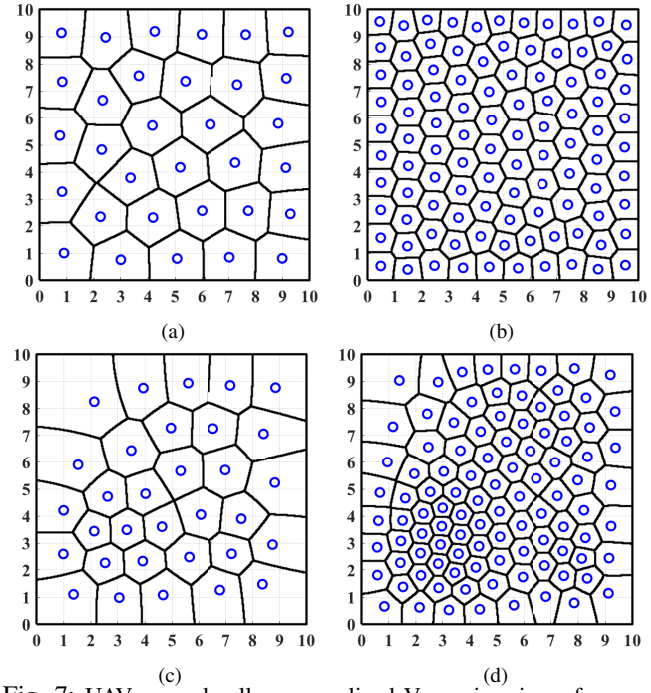

(a) (b) (c) (d)

Fig. 7: UAV ground cells, generalized Voronoi regions, for $\alpha = 2$ and a uniform probability density function (a) with 32 UAVs, (b) with 100 UAVs, and a non-uniform density (c) with 32 UAVs, (d) with 100 UAVs.

is the nth generalized Voronoi region [31, Chap. 3]. Here, we denote the weights as in (12) by the positive numbers $a_n = h_n^{-\frac{\kappa}{\gamma}}$ and $b_n = h_n^{2-\frac{\kappa}{\gamma}}$ and define a *Möbius tessellations* [26], [49]. As shown below, the bisectors of Möbius tessellation are circles or lines in $\mathbb{R}^2$. The nth Voronoi region is defined by $N-1$ inequalities, which can be written as the intersection of the $N-1$ *dominance regions* of $\mathbf{q}_n$ over $\mathbf{q}_m$, given by

$$\mathcal{V}_{nm} = \left\{ \boldsymbol{\omega} \in \Omega \;\middle|\; a_n \left\|\mathbf{q}_n - \boldsymbol{\omega}\right\|^2 + b_n \leq a_m \left\|\mathbf{q}_m - \boldsymbol{\omega}\right\|^2 + b_m \right\}. \tag{34}$$

If $h_n = h_m$, then $a_n = a_m$ and $b_n = b_m$, such that $\mathcal{V}_{nm}$ is the left half-space between $\mathbf{q}_n$ and $\mathbf{q}_m$. For $h_m > h_n (a_n > a_m)$, we can rewrite the inequality for each dominance region $\mathcal{V}_{nm}$ as circular regions $\left\|\boldsymbol{\omega} - \mathbf{c}_{n,m}\right\|^2 \leq r_{n,m}$ with center point $\mathbf{c}_{n,m}$ and radius $r_{n,m}$ as given in Theorem 1. If $h_m < h_n$, then the dominance region is the complement of the disc with respect to Ω. For more details see [50, App. A].

Appendix B
Proof of Theorem 1

For the homogeneous case with fixed common height $h = h_n$, the distortion function d is given by a non-decreasing continuous and positive function in the Euclidean distance $r = \left\|\mathbf{q} - \boldsymbol{\omega}\right\|$ as

$$d(\mathbf{q}, \boldsymbol{\omega}) = f_{\gamma,\kappa}(\left\|\mathbf{q} - \boldsymbol{\omega}\right\|, h) = (\left\|\mathbf{q} - \boldsymbol{\omega}\right\|^2 + h^2)^{\gamma} / h^{\kappa}. \tag{35}$$

Since we assume a uniform density, we have $\lambda(\omega) = 1/A$ for all $\omega \in \Omega$.

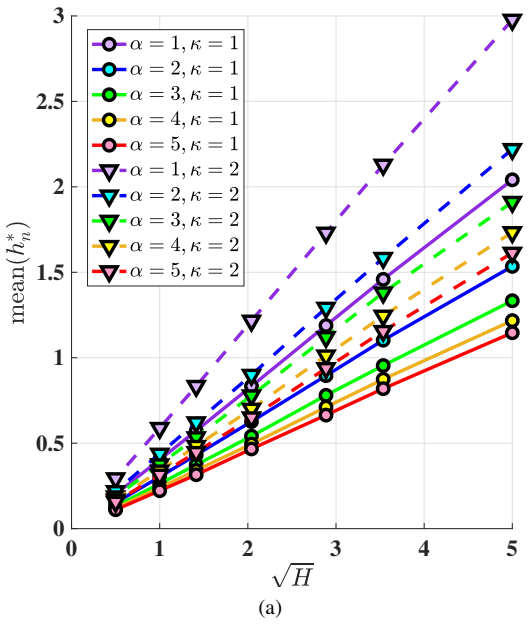

(a)

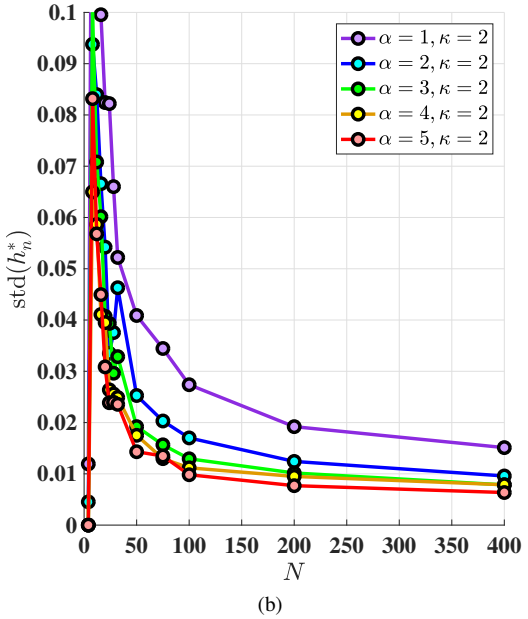

(b)

Fig. 8: (a) Optimal common height for $\alpha = 1, 2, 3, 4, 5$ and $\kappa = 1, 2$ over $\sqrt{H} = \sqrt{A/N}$, derived with brute force optimization and analytically by Theorem 1. (b) The variance (standard deviation) of all N optimal heights converge exponentially fast in N for κ = 2.

The optimal deployment problem with $h = h_n$ has centroidal ground positions given by [43]

$$\int_{\mathcal{V}_n^*} \frac{(\|\mathbf{q}_n^* - \boldsymbol{\omega}\|^2 + h^{*2})^\gamma}{h^{*\kappa}} d\boldsymbol{\omega} = \min_{\mathbf{q}\in \mathrm{Clos}(\mathcal{V}_n^*)} \int_{\mathcal{V}_n^*} \frac{(\|\mathbf{q} - \boldsymbol{\omega}\|^2 + h^{*2})^\gamma}{h^{*\kappa}} d\boldsymbol{\omega}, \tag{36}$$

where $\mathrm{Clos}(\mathcal{V}_n^*)$ denotes the convex closure of the set $\mathcal{V}_n^*$. Unfortunately, there is no closed form expression for arbitrary γ. However, asymptotically ($N \to \infty$, high-resolution) it is known that the optimal Voronoi regions are congruent to the regular Hexagon, i.e., $\mathcal{V}_n^* \sim \mathcal{H}_n$ [43]. Hence, from the conditions (26) and (27), we obtain a local critical common height, if and only if

$$z = h^{*2} = \frac{\frac{1}{A}\int_{\mathcal{H}_n}(\|\boldsymbol{\omega} - \mathbf{q}_n^*\|^2 + h^{*2})^\gamma d\boldsymbol{\omega}}{\frac{2\gamma}{\kappa A}\int_{\mathcal{H}_n}(\|\boldsymbol{\omega} - \mathbf{q}_n^*\| + h^{*2})^{\gamma-1} d\boldsymbol{\omega}}. \tag{37}$$

We know that $h^* > 0$ and hence $h^{*2} = z > 0$ is associated to only one height. Since the optimal ground positions are all centroidal and the regions $\mathcal{V}_n$ are all congruent, asymptotically we have

$$\int_{\mathcal{H}_n}(\|\boldsymbol{\omega}-\mathbf{q}_n^*\|^2+z)^\gamma d\omega \sim \int_{\mathcal{H}}(\|\boldsymbol{\omega}\|^2+z)^\gamma d\boldsymbol{\omega} = \tilde{M}_{\mathcal{H}}(2\gamma, H). \tag{38}$$

Here, we centered the Hexagon $\mathcal{H}$ such that the centroids are at the origin $\mathbf{q}^* = \mathbf{0}$. The integral $\tilde{M}_{\mathcal{H}}(2\gamma, H)$ denotes a distorted polar moment of a hexagon with area $H = \mu(\mathcal{H}) = \mu(\mathcal{V}_n^*) = A/N$. More precisely, the additive distortion z creates a polynomial of different *polar moments of the hexagon*. Since we need to identify the distortion z which achieves equality in (37), we have to calculate the polar moments, which determine the polynomial coefficients of

$$g_\gamma(z) = \int_{\mathcal{H}} \frac{2\gamma}{\kappa} z(\|\boldsymbol{\omega}\|^2+z)^{\gamma-1} d\boldsymbol{\omega} - \int_{\mathcal{H}}(\|\boldsymbol{\omega}\|^2+z)^\gamma d\boldsymbol{\omega} = 0. \tag{39}$$

Note that both integrals are strictly positive increasing and continuous functions in $z \geq 0$ for any real-valued $\gamma \geq 1$. Since for $z = 0$ the first integral is vanishing and the second one is not, there can exist only one $z > 0$ for which the difference vanishes. Such a z exists, since for $2\gamma/\kappa > 1$ the first integral increases faster in z compared with the second one. Hence, there exists only one optimal common height $h^* = \sqrt{z}$. Furthermore, the kernel integral only depends on the radius $\|\boldsymbol{\omega}\|$ and since the hexagon $\mathcal{H}$ consists of 12 right-angled triangles Δ, which are identical up to a rotation around the origin, as shown in Fig. 9, we derive the equivalent condition for (39):

$$\int_\Delta \left(\frac{2\gamma}{\kappa} z(\|\boldsymbol{\omega}\|^2 + z)^{\gamma-1} - (\|\boldsymbol{\omega}\|^2 + z)^\gamma \right) d\boldsymbol{\omega} = 0. \tag{40}$$

Hence, we only have to deal with polar moments of the triangle Δ. To calculate solutions for specific values of γ, we need to explicitly calculate the integrals. The areas of the hexagon and triangles in terms of the radius r of the inscribed circle, are respectively,

$$H = \mu(\mathcal{H}) = 12\int_\Delta d\boldsymbol{\omega} = 6r^2 \tan\frac{\pi}{6} = 2\sqrt{3}r^2, \;\; \mu(\Delta) = \frac{H}{12}, \tag{41}$$

see for example [51, p. 4.5.3] and Fig. 9. Note that the length of the edges are the same as the outer radius $R = \frac{2r}{\sqrt{3}}$. However, for arbitrary $\gamma \geq 1$, we need general orders of the moments $M_\Delta(\epsilon, H) = \int_\Delta \|\boldsymbol{\omega}\|^\epsilon \, d\boldsymbol{\omega}$. Since $\|\boldsymbol{\omega}\|^\epsilon = f(\rho, \phi) = \rho^\epsilon$, is continuous in the radius ρ and angle ϕ, we can parameterize the integral in polar coordinates, as shown in Fig. 9a, to derive

$$M_\Delta(\epsilon, H) = \frac{r^{\epsilon+2}}{2\epsilon+4}\beta\left(\frac{\epsilon+3}{2}\right) = \left(\frac{H}{2\sqrt{3}}\right)^{\epsilon+2}\frac{1}{2\epsilon+4}\beta\left(\frac{\epsilon+3}{2}\right). \tag{42}$$

With the integral representation in [36, 8.375(2)], for odd $\epsilon =$

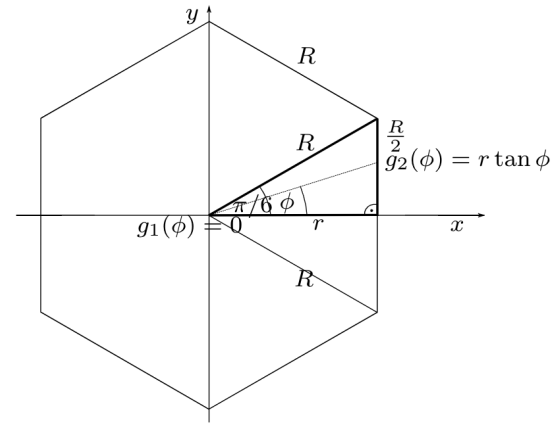

(a)

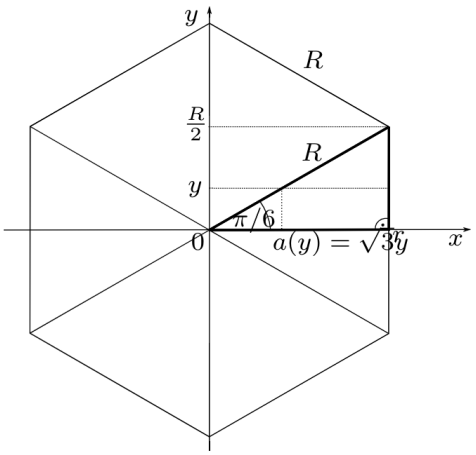

(b)

Fig. 9: Hexagon parameterization in 12 right triangles Δ with (a) Polar and (b) Cartesian coordinates.

$2n-1$, we get the expression

$$\beta(n+1) = (-1)^n \ln 2 + \sum_{i=1}^{n} \frac{(-1)^{i+n}}{i} \quad , \quad n \in \mathbb{N}_+. \tag{43}$$

Unfortunately, a closed-form expression for $\beta(n+1/2)$ or $\beta(x)$ is difficult to derive since they are given in terms of the *Gamma* or *Riemann-Zeta function*. However, we can use the Cartesian parameterization to derive the even moments for $\epsilon = 0, 2, 4, 6$.

$$\begin{aligned} M_\Delta(0,H) &= \frac{H}{12}, M_\Delta(2,H) = \frac{5H^2}{216\sqrt{3}}, \\ M_\Delta(4,H) &= \frac{7H^3}{270\cdot 9}, M_\Delta(6,H) = \frac{83H^4}{72\cdot 35\cdot 27\sqrt{3}}, \end{aligned} \tag{44}$$

where we used (41) for H. For more details on the derivation of even moments of inertia see [50, App. C]. With (40), this yields to the global common height for $\gamma = \kappa = 1$

$$\begin{aligned} h^*(1,H) \sim \sqrt{z} &= \sqrt{\frac{\kappa}{2-\kappa}\frac{M_\Delta(2,H)}{M_\Delta(0,H)}} = c(1)\sqrt{H}, \\ c(1) &= \sqrt{\frac{5}{18\sqrt{3}}} \approx \sqrt{0.1603}. \end{aligned} \tag{45}$$

For $\gamma = 2$ and $3 \geq \kappa \geq 1$, we obtain from (40) a quadratic equation in z:

$$g_2(z) = \int_\Delta \left(\frac{4-\kappa}{\kappa} z^2 + \frac{4-2\kappa}{\kappa} z \left\|\boldsymbol{\omega}\right\|^2 - \left\|\boldsymbol{\omega}\right\|^4 \right) d\boldsymbol{\omega}. \tag{46}$$

Solving for z and taking the square root, we obtain the optimal height and scaling constant

$$\begin{aligned} &h^*(2,\kappa,H) = c(2,\kappa)\sqrt{H} \text{ with} \\ &c(2,\kappa) = \sqrt{\frac{\sqrt{\frac{(172-43\kappa)\kappa}{5} + 100} - 10 + 5\kappa}{18\sqrt{3}(4-\kappa)}}. \end{aligned} \tag{47}$$

Finally, for $\gamma = 3$ and $5 \geq \kappa \geq 1$, we get a cubic equation

$$\begin{aligned} g_3(z) =& z^3 \frac{6-\kappa}{\kappa} \int_\Delta + z^2 \frac{12-3\kappa}{\kappa} \int_\Delta \left\|\boldsymbol{\omega}\right\|^2 \\ &+ z \frac{6-3\kappa}{\kappa} \int_\Delta \left\|\boldsymbol{\omega}\right\|^4 - \int_\Delta \left\|\boldsymbol{\omega}\right\|^6. \end{aligned} \tag{48}$$

Inserting the moments (44), we get as valid solutions of the cubic equation [52, (3.8.2)] as

$$\begin{aligned} &z_1 = s_1^{1/3} + s_2^{1/3} - \frac{5H(4-\kappa)}{18\sqrt{3}(6-\kappa)} \quad \text{with} \\ &s_1 = p + \sqrt{q^3+p^2}, \; s_2 = p - \sqrt{q^3+p^2}, \end{aligned} \tag{49}$$

where we have

$$\begin{aligned} q &= \frac{43\kappa^2 - 344\kappa + 16}{4860(6-\kappa)^2} H^2, \\ p &= \frac{-143360 + 16728\kappa + 444\kappa^2 - 37\kappa^3}{612360\sqrt{3}(6-\kappa)^3} H^3. \end{aligned} \tag{50}$$

Note that the discriminant $q^3 + p^2 > 0$ for $1 \leq \kappa \leq 5$ and every $H > 0$. Therefore, there exists only one real-valued solution, given by z_1. Then, asymptotically, the optimal height for H and $\gamma = 3$ can be derived as $h^*(3,\kappa,H) = c(3,\kappa)\sqrt{H}$ with constant $c(3,\kappa)$ as in (29). Asymptotically, the minimal average distortion is given by (25) as

$$\begin{aligned} \bar{P}^*(\gamma,H) &\sim \frac{N}{A} \int_{\mathcal{H}} \frac{(\left\|\boldsymbol{\omega}\right\|^2 + (h^*(\gamma,H))^2)^\gamma}{h^*(\gamma,H)} d\boldsymbol{\omega} \\ &= \frac{12}{H} \int_\Delta \frac{(\left\|\boldsymbol{\omega}\right\|^2 + (h^*(\gamma,H))^2)^\gamma}{h^*(\gamma,H)} d\boldsymbol{\omega}. \end{aligned} \tag{51}$$

For $\gamma = 1,\ 2,\ 3$, using (45) and the moments (44), after some calculations, we get (52), (53), and (54). Normalizing by the maximal directivity will give the final result [50, App. B].

References

[1] J. Guo, P. Walk, and H. Jafarkhani, "Quantizers with parameterized distortion measures," in *Data Compression Conf. (DCC)*, Mar. 2019.

[2] X. Li, H. Yao, J. Wang, X. Xu, C. Jiang, and L. Hanzo, "A near-optimal UAV-aided radio coverage strategy for dense urban areas," *IEEE Transactions on Vehicular Technology*, vol. 68, no. 9, pp. 9098–9109, Sep. 2019.

[3] J. Wang, C. Jiang, Z. Han, Y. Ren, R. G. Maunder, and L. Hanzo, "Taking drones to the next level: Cooperative distributed unmanned-aerial-vehicular networks for small and mini drones," *IEEE Vehicular Technology Magazine*, vol. 12, no. 3, pp. 73–82, Sep. 2017.

[4] X. Li, H. Yao, J. Wang, S. Wu, C. Jiang, and Y. Qian, "Rechargeable multi-UAV aided seamless coverage for QoS-guaranteed IoT networks," *IEEE Internet of Things Journal*, vol. 6, no. 6, pp. 10 902–10 914, Dec. 2019.

$$\bar{P}^*(1,1,H) \sim \frac{12}{H}\left[\sqrt{\frac{18\sqrt{3}}{5H}}\int_{\Delta}\|\boldsymbol{\omega}\|^2\,d\boldsymbol{\omega} + \sqrt{\frac{5H}{18\sqrt{3}}}\int_{\Delta} d\boldsymbol{\omega}\right] = \sqrt{\frac{10H}{9\sqrt{3}}} \approx 0.8H^{\frac{1}{2}} \tag{52}$$

$$\bar{P}^*(2,\kappa,H) \sim \left(\frac{14}{405c(2,\kappa)} + \frac{5c(2,\kappa)}{9\sqrt{3}} + c^3(2,\kappa)\right)H^{\frac{3}{2}} \tag{53}$$

$$\bar{P}^*(3,\kappa,H) \sim \left(\frac{83}{195\cdot 27c(3,\kappa)} + \frac{14c(3,\kappa)}{135} + \frac{5c^3(3,\kappa)}{9\sqrt{3}} + c^5(3,\kappa)\right)H^{\frac{5}{2}} \tag{54}$$

[5] J. Wang, C. Jiang, Z. Wei, C. Pan, H. Zhang, and Y. Ren, "Joint UAV hovering altitude and power control for space-air-ground IoT networks," *IEEE Internet of Things Journal*, vol. 6, no. 2, pp. 1741–1753, Apr. 2019.

[6] P. Zhan, K. Yu, and A. L. Swindlehurst, "Wireless relay communications with unmanned aerial vehicles: Performance and optimization," *IEEE Transactions on Aerospace and Electronic Systems*, vol. 47, no. 3, pp. 2068–2085, Jul. 2011.

[7] Y. Zeng, Q. Wu, and R. Zhang, "Accessing from the sky: A tutorial on uav communications for 5g and beyond," Mar. 2019. arXiv: 1903.05289.

[8] B. Galkin, J. Kibilda, and L. A. DaSilva, "Backhaul for low-altitude UAVs in urban environments," in *ICC*, May 2018.

[9] M. M. Azari, F. Rosas, and S. Pollin, "Reshaping cellular networks for the sky: Major factors and feasibility," in *2018 IEEE International Conference on Communications (ICC)*, Oct. 2018. arXiv: 1710.11404v2.

[10] H. Shakhatreh and A. Khreishah, "Maximizing indoor wireless coverage using UAVs equipped with directional antennas," May 2017. arXiv: 1705.09772v1.

[11] Z. Yang, C. Pan, M. Shikh-Bahaei, W. Xu, M. Chen, M. Elkashlan, and A. Nallanathan, "Joint altitude, beamwidth, location, and bandwidth optimization for UAV-enabled communications," *IEEE Commun. Lett.*, vol. 22, no. 8, pp. 1716–1719, Aug. 2018.

[12] H. He, S. Zhang, Y. Zeng, and R. Zhang, "Joint altitude and beamwidth optimization for UAV-enabled multiuser communications," *IEEE Commun. Lett.*, vol. 22, no. 2, pp. 344–347, Feb. 2018.

[13] M. Mozaffari, W. Saad, M. Bennis, and M. Debbah, "Efficient deployment of multiple unmanned aerial vehicles for optimal wireless coverage," *IEEE Commun. Lett.*, vol. 20, no. 8, pp. 1647–1650, Aug. 2016.

[14] Z. Yang, C. Pan, K. Wang, and M. Shikh-Bahaei, "Energy efficient resource allocation in UAV-enabled mobile edge computing networks," 2019. arXiv: 1902.03158.

[15] M. Alzenad, A. El-Keyi, F. Lagum, and H. Yanikomeroglu, "3D placement of an unmanned aerial vehicle base station (UAV-BS) for energy-efficient maximal coverage," *IEEE Trans. Wireless Commun.*, vol. 6, no. 4, pp. 434–437, Aug. 2017.

[16] A. Al-Hourani, S. Kandeepan, and S. Lardner, "Optimal LAP altitude for maximum coverage," *IEEE Wireless Communications Letters*, vol. 3, no. 6, pp. 569–572, Dec. 2014.

[17] J. Guo, E. Koyuncu, and H. Jafarkhani, "A source coding perspective on node deployment in two-tier networks," *IEEE Trans. Commun.*, vol. 66, no. 7, pp. 3035–3049, Jul. 2018.

[18] E. Koyuncu, R. Khodabakhsh, N. Surya, and H. Seferoglu, "Deployment and trajectory optimization for UAVs: A quantization theory approach," in *2018 IEEE WCNC*, Apr. 2018. arXiv: 1708.08832v5.

[19] J. Lyu and R. Zhang, "Network-connected UAV: 3-D system modeling and coverage performance analysis," *IEEE Internet of Things Journal*, vol. 6, no. 4, pp. 7048–7060, Aug. 2019.

[20] P. Jankowski-Mihułowicz, W. Lichoń, and M. Węglarski, "Numerical model of directional radiation pattern based on primary antenna parameters," *Int. J. of Electronics and Telecommunications*, vol. 61, no. 2, pp. 191–197, Jul. 2015.

[21] C. A. Balanis, *Antenna Theory: Analysis and Design*, 3rd ed. Wiley-Interscience, 2005.

[22] E. Koyuncu and H. Jafarkhani, "On the minimum distortion of quantizers with heterogeneous reproduction points," *Data Compression Conference*, Mar. 2016.

[23] ——, "On the minimum average distortion of quantizers with index-dependent distortion measures," *IEEE Transactions on Signal Processing*, vol. 65, no. 17, pp. 4655–4669, Sep. 2017.

[24] A. Gusrialdi, S. Hirche, T. Hatanaka, and M. Fujita, "Voronoi based coverage control with anisotropic sensors," in *American Control Conference*, IEEE, Jun. 2008.

[25] M. Moarref and L. Rodrigues, "An optimal control approach to decentralized energy-efficient coverage problems," 3, vol. 47, Elsevier BV, Aug. 2014, pp. 6038–6043.

[26] J.-D. Boissonnat, C. Wormser, and M. Yvinec, "Curved voronoi diagrams," in *Effective Computational Geometry for Curves and Surfaces*. Springer, 2007.

[27] J. Guo and H. Jafarkhani, "Sensor deployment with limited communication range in homogeneous and heterogeneous wireless sensor networks," *IEEE Trans. Wireless Commun.*, vol. 15, no. 10, pp. 6771–6784, Oct. 2016.

[28] ——, "Movement-efficient sensor deployment in wireless sensor networks," *IEEE Trans. Wireless Commun.*, vol. 18, pp. 3469–3484, Jul. 2019.

[29] M. T. Nguyen, L. Rodrigues, C. S. Maniu, and S. Olaru, "Discretized optimal control approach for dynamic multi-agent decentralized coverage," in *IEEE International Symposium on Intelligent Control (ISIC)*, Sep. 2016.

[30] S. Karimi-Bidhendi, J. Guo, and H. Jafarkhani, "Using quantization to deploy heterogeneous nodes in two-tier wireless sensor networks," Jul. 2019. arXiv: 1901.06742.

[31] A. Okabe, B. Boots, K. Sugihara, and S. N. Chiu, *Spatial Tessellations: Concepts and Applications of Voronoi Diagrams*, 2nd ed. John Wiley & Sons, 2000.

[32] K. Venugopal, M. C. Valenti, and R. W. Heath, "Device-to-device millimeter wave communications: Interference, coverage, rate, and finite topologies," *IEEE Trans. Wireless Commun.*, vol. 15, no. 9, pp. 6175–6188, Sep. 2016.

[33] A. Goldsmith, *Wireless Communications*. Cambridge University Press, 2005.

[34] *Guidelines for evaluation of radio interface technologies for IMT-advanced*, ITU recommendation M.2135-1, Geneva, Switzerland: ITU, 2009.

[35] A. Al-Hourani and K. Gomez, "Modeling cellular-to-UAV path-loss for suburban environments," *IEEE Wireless Communications Letters*, vol. 7, no. 1, pp. 82–85, Feb. 2018.

[36] I. S. Gradshteyn and I. M. Ryzhik, *Table of Integrals, Series, and Products*, 8th ed., A. Jeffrey and D. Zwillinger, Eds. Academic Press, 2015.

[37] M. Mozaffari, W. Saad, M. Bennis, and M. Debbah, "Unmanned aerial vehicle with underlaid device-to-device communications: Performance and tradeoffs," *IEEE Trans. Wireless Commun.*, vol. 15, no. 6, pp. 3949–3963, Jun. 2016.

[38] Y. Zeng, J. Xu, and R. Zhang, "Energy minimization for wireless communication with rotary-wing UAV," *IEEE Transactions on Wireless Communications*, vol. 18, no. 4, pp. 2329–2345, Apr. 2019.

[39] J. Cortés, S. Martínez, and F. Bullo, "Spatially-distributed coverage optimization and control with limited-range interactions," *ESAIM*, vol. 11, no. 4, pp. 691–719, Sep. 2005.

[40] A. David and V. Sergei, "How slow is the k-means method?" In *The Twenty-second Annual Symposium on Computational Geometry.*, Jan. 2006, pp. 144–153.

[41] D. Aloise, A. Deshpande, P. Hansen, and P. Popat, "NP-hardness of euclidean sum-of-squares clustering," *Machine Learning*, vol. 75, no. 2, pp. 245–248, 2009.

[42] J. Guo, P. Walk, and H. Jafarkhani, "Quantizers with parameterized distortion measures," Nov. 2018. arXiv: 1811.02554.

[43] Q. Du, V. Faber, and M. Gunzburger, "Centroidal voronoi tessellations: Applications and algorithms," *SIAM Review*, vol. 41, no. 4, pp. 637–676, Oct. 1999.

[44] W. H. Press, S. A. Teukolsky, W. T. Vetterling, and B. P. Flanner, *Numerical Recipes: The Art of Scientific Computing*, 3rd ed. Cambridge University Press, 2007.

[45] K. O. Geddes, S. R. Czapor, and G. Labahn, *Algorithms for Computer Algebra*. Kluwer Academic Publishers, 1992.

[46] M. J. Golin and H. S. Na, "On the average complexity of 3d-voronoi diagrams of random points on convex polytopes," *Computational Geometry*, vol. 25, no. 3, pp. 197–231, Jul. 2003.

[47] F. Aurenhammer and H. Edelsbrunner, "An optimal algorithm for constructing the weighted voronoi diagram in the plane," *Pattern Recognition*, vol. 17, no. 2, pp. 251–257, 1984.

[48] Z. Gaspar and T. Taranai, "Upper bound of density for packing of equal circles in special domains in the plane," *Periodica Polytechnica Civil Engineering*, vol. 44, no. 1, pp. 13–32, Apr. 2000.

[49] J.-D. Boissonnat and M. I. Karavelas, "On the combinatorial complexity of euclidean voronoi cells and convex hulls of d-dimensional spheres," *INRIA*, Jul. 2002.

[50] J. Guo, P. Walk, and H. Jafarkhani, "Optimal deployments of uavs with directional antennas for a power-efficient coverage," *arixv.org*, 2019. arXiv: 1911.07463.

[51] D. Zwillinger, *Standard Mathematical Tables and Formulae*, 31st ed. CRC, 2003.

[52] M. Abramowitz and I. A. Stegun, *Handbook of Mathematical Functions with Formulas, Graphs, and Mathematical Tables*. Dover Publications Inc., 1964.